3D SEISMIC ANALYSIS OF CENOZOIC SLOPE DEPOSITS AND FLUID FLOW PHENOMENA ALONG THE NIGERIAN TRANSFORM MARGIN

[1],[2] Oluwatobi Olobayo & [1]Mads Huuse,

[1]Department of Earth and Environmental Sciences, The University of Manchester, Manchester M13 9 PL, England, UK

[2]Data, Digital and Technology, UK

Corresponding author oluwatobiolobayo@yahoo.com

ABSTRACT

High-resolution 3D seismic data covering an area of 2,845 km^2 provide new insights on slope deposits and fluid-flow phenomena along the Nigerian Transform Margin, focusing on the ~ 2 km thick Cenozoic post-transform succession. The study documents large-scale mass-transport complexes, deep-water channel complexes, sediment waves, and a wide range of fluid flow phenomena. The focused fluid flow phenomena include pockmarks, vertical pipes, seabed mounds and gas-hydrate related bottom simulating reflections. They are observed from Pliocene-aged sediments and distributed above structural highs, regional faults and active and relic deep-water channels in the eastern part of the study area, closest to the Niger Delta cone. The identified fluid flow features could be indicative of an active petroleum system in the deeper subsurface, and fluids could have migrated along planes of deep-seated, regional faults. The mass- transport deposits are mapped at multiple levels and the volume of failed sediments increased through time such that they constitute very significant portion of the entire stratigraphic succession (up to 25%) within the western part of the study area. The repeated and increased volume of mass transport deposit in the area is attributed to increased rate of sedimentation through time, slope gradient and probably increasing amplitude of sea level change during the late Cenozoic. The presence of repeated mass-transport deposits and fluid flow phenomena on the Nigeria Transform Margin has implications for installations of offshore facilities as they constitute potential geohazards. The study documents, for the first time, polygonal fault systems offshore Nigeria, adding to the global inventory of polygonally-faulted claystones, and suggesting a more oceanic dominated mudstone sedimentation than nearer the Niger Delta.

INTRODUCTION

Significant interest and exploration activity along the equatorial conjugate margins led to acquisition of a 2,845 km^2 of high-resolution 3D seismic ('Geostreamer') data from the Nigeria Transform Margin in 2010 by Petroleum Geo-Services (PGS) in cooperation with the Department of Petroleum Resources (DPR) of Nigeria. It was acquired, to confirm the presence of Cretaceous play fairways already discovered along the West African Transform and Brazilian margins (Fig. 1). The survey area falls within the Dahomey-Benin basin, part of the east-west aligned sedimentary basins formed during the Late Cretaceous rifting of the African and South American plates (Brownfield & Charpentier 2006; Greenhalgh *et al.,* 2011).

The study area is located in the western part of Nigeria within the West Africa Transform Margin (WATM) covering Oil Prospecting License 312, 313 and 314 (OPL) (Fig. 1b). It is bounded to the north by Aje field and Ogo discovery within OML 113 and OPL 310 respectively, to the west by the Hihon and Fifa fields and to the east by the Niger-Delta basin (Fig. 1a). Water depths recorded in the area is between 1.5 and 3.8 km. The studied interval is bounded at the base and top by the Top Albian unconformity and present-day seabed respectively, which formed the thick overburden for underlying Cretaceous source and reservoir rocks (Fig. 2). High-resolution, three-dimensional (3D) seismic data facilitated detailed study of series of seabed and subsurface features. These features include; soft-sediment deformation and remobilization products (MTDs), depositional elements and fluid-flow features, which represent significant part of the basin evolution and fluid-flow history.

Mass-transport deposits (MTDs), deep-water channels, and sediment waves form important components of the continental slope of the Nigeria Transform Margin. Mass-transport deposits (MTDs) are common in deep-water settings and easily recognised on seismic sections due to their chaotic internal character, large size, extensive nature and distinctive external geometry (Shipps *et al.,* 2011). Integration of 2D, 3D seismic data, side-scan sonar, multibeam bathymetry, well data and outcrop studies have improved understanding of MTDs in the last few decades. This has helped the study of their geometries, distribution, evolution and relationship with other depositional elements (Nissen *et al.,* 1999; Posamentier & Kolla 2003; Moscardelli *et al.,* 2006; Shipps *et al.,* 2011). The MTDs form up to 40% of the entire succession studied with high-level of preservation of most of its components such as head scarps, lateral margins, deformed blocks, ramps etc, used as kinematic indicators to unravel the evolution and . direction of translation of failed sediments (Bull *et al,* 2009). Repeated occurrence of mass-transport deposits in the area suggests an unstable slope throughout the Cenozoic and as such very critical to exploration and production as they would form potential geohazards for offshore facilities installations and subsequent drilling (Martinez *et al.,* 2011; Posamentier & Martinsen 2011). The association of MTDs with turbidites, which constitute significant target for deep-water drilling, suggest the need to map their lateral and vertical distribution and also to understand their morphology (Shipp *et al.,* 2011; Nelson *et al.,* 2011).

Fluid flow features form as a result of fluid movement within the sedimentary basin; this could be water, gas or oil or a combination of the three; represented as high or low amplitude anomalies on the seismic data (Judd & Hovland 2007; Cartwright *et al.,* 2007; Løseth *et al.,* 2009). A wide range of fluid flow features occur in the geologic record either on the present-day seabed or in the subsurface; they include sandstone intrusions, mud volcanoes, pockmarks, pipes, chimneys, bottom simulating reflections (BSRs), carbonate mounds, diagenetic boundaries and polygonal faults (Shipley *et al.,* 1979; Cartwright 1994; Cunningham & Lindholm 2000; Graue 2000; Løseth *et al.,* 2001; 2011; Davies 2003; Cartwright *2007;* Huuse *et al.,* 2010; Andersen 2012). The fluid source could be either thermogenic, biogenic or both (Gay *et al.,* 2006a; Judd & Hovland 2007). We observe both seabed and subsurface fluid flow features such as pockmarks, pipes and BSRs, and these could be indicative of active petroleum system in the area. Hydrocarbon generation within the basin began in the Late Miocene

and continued till date, although generation started much earlier in neighbouring basins (Brownfield & Charpentier 2006).

The aim of this paper is to document the occurrence of mass-transport deposits and other depositional elements and fluid flow features along the Nigeria Transform Margin. This includes details of their spatial distribution, mode of occurrence as well as their usefulness in understanding the evolution and fluid flow of the basin. Main results from the analysis of 3D seismic data include; (1) sub-division of the post-transform section into five (5) main seismic units separated by major unconformities and surfaces; (2) spatial and temporal distribution of mass transport deposits through time; (3) documentation of fluid-flow features which includes pockmarks, pipes, furrows, BSRs restricted in the eastern part of the area and their relationship with structural highs, deep-water channels and regional faults; and (4) the first documentation of polygonal faults along the Nigeria Transform Margin.

GEOLOGICAL SETTING

The study area is located within the Dahomey-Benin basin, which stretches from southeastern Ghana to southwestern Nigeria (Obaje 2009). The basin is separated from the Niger Delta by the Okitipupa ridge (Obaje 2009). This basin forms part of the east-west aligned basins within the Gulf of Guinea. These basins were initiated during the Late Jurassic rifting between the African and South American plates; and are characterized by transform and wrench faults formed during the separation. Which results in similarities between the structural and stratigraphic elements within these basins (Greenhalgh *et al.,* 2011). The Nigerian Transform Margin (study area) and the other basins within the Gulf of Guinea are in contrast to other passive-margin basins such as the Lower Congo and Angola basins mainly by the influence of transform tectonics and by the absence of salt tectonics (MacGregor *et al.,* 2003).

Basin evolution spanned three phases, separated by major unconformities (Fig. 2). These include; pre-transform or pre-rift (Late Proterozoic to Late Jurassic), syn-transform or syn-rift (Late Jurassic to Early Cretaceous) and post- transform or post-rift (Late Cretaceous to Holocene) (Brownfield & Charpentier 2006). The Gulf of Guinea formed at the end of Late Jurassic to Early Cretaceous time and was characterized by transform and block faulting above a regionally extensive Paleozoic basin during the breakup of the north Atlantic (separation of North America from Europe and Africa) that started during the Late Permian to Early Triassic time (Ziegler 1988). Thick continental crust of the African and South American continental plates began to breakup in Early Albian time and formed the basins separated by transform faults (Blarez & Mascle 1988). The culmination of transform tectonism in the middle to Late Albian time coincided with initial breakup of oceanic crust along the continents and formed the Gulf of Guinea initially as an anoxic oceanic basin; but by the beginning of Campanian, the Gulf of Guinea and the rest of the Atlantic Ocean had become an open-marine seaway (Brownfield & Charpentier 2006).

The stratigraphic section of the basin has been subdivided based on the three stages of tectonic evolution which includes; Precambrian to Early Cretaceous rocks for pre-transform, Early Cretaceous to Late Albian sediments for syn-transform and the Cenomanian to Holocene sediments representing the post-transform stage (Brownfield & Charpentier 2006). For the purpose of this study, we will only summarize the post-transform succession, which the studied interval encompasses (Fig. 2). The Top Albian unconformity marked the end of the syn-transform phase, followed by thermal subsidence that continued till present day (Greenhalgh *et al.,* 2011). In the middle to Late Cretaceous, deeply incised canyons were eroded into the shelf during relative sea- level falls and transported sediments into the basin as large turbidite fans, which are main reservoir targets along the transform margin (Fig. 2) (Brownfield & Charpentier 2006; Greenhalgh *et al.,* 2011). These sandstones were deposited within the

Araromi and Agwu Shale Formation, which may have formed source rocks and seals for the reservoirs (Fig. 2) (Borsato *et al.,* PGS).

Non-marine to marginal marine conditions prevailed during the middle Cretaceous and is expected to contain gas-prone source rocks (MacGregor 2003; Brownfield & Charpentier 2006). Sediments deposited during the Late Cretaceous in the basin were divided two main stratigraphic units; the Abeokuta and Araromi Formations (Obaje 2009). Sandstone of the Araromi Formations forms the reservoir sands of the Aje and Seme fields in Nigeria and Benin respectively (Fig. 2). Tertiary rocks unconformably overlie Cretaceous rocks and comprises of Paleocene to Eocene marine shales of the Imo Shale Formation and interbedded with Ameki Formation sandstones in the study area (Fig. 2). A major Oligocene-Miocene unconformity separated the Early Tertiary succession from Miocene marine rocks (Fig. 2) (Brownfield & Charpentier 2006; Borsato *et al.,* PGS). Fluid flow features observed are concentrated within Pliocene to Recent sediments.

Generation and migration of hydrocarbon within the Dahomey-Benin basin started during the Miocene and continued till present-day (MacGregor 2003; Brownfield & Charpentier 2006).

DATASET AND METHODS

Dataset

A 2,845 km^2 of GeoStreamer, 3D high-resolution seismic data from the West African Transform Margin was provided by Petroleum Geo-services (PGS). Seismic data covers Oil Prospecting Licence (OPL) 312, 313 and 314 (Fig. 3). The 3D seismic data is pre-stack time migrated with a bin size (inline and crossline spacing) of 12.5 m x 12.5 m. Data quality is very good except interval below the channel complex in the eastern part of the study area. Water depth ranges between 3000 – 3800 ms two-way-time (TWT) and seismic data goes down to six seconds TWT. The seismic data is zero- phase processed with normal SEG polarity such that an increase in acoustic impedance is represented by positive amplitude = red peaks = hard reflections. Frequency, horizontal and vertical resolutions were calculated for each unit assuming an average seismic velocity (*V)* of 2000 m/s (Tab. 1). Unfortunately, no well data was available for the study making it difficult to ascertain actual lithology and horizon and sequence ages where based on the nearby Aje Field (Appen).

Methods

The study area was divided into two areas for ease of description: area 1 - the eastern part (fluid flow zone) and area 2 (mass-transport deposit zone). Each of the areas represents approximately the limits of these features (Fig. 3). 6 major horizons were mapped using 2D and 3D tracking using Schlumberger Petrel. These horizons were matched from horizons in the survey north of the study area in OML133 (Aje field) therefore ages of horizons are based on previous interpretation (Fig. 1b; Appendix 1.2 & 1.3). Seismic stratigraphic techniques based on seismic facies, reflection continuity and terminations were also applied to map the area (Mitchum *et al.,* 1977).

Several horizons between the main horizons were also produced from horizon stacking using Paleoscan to image features of interest on individual horizons. Time surface maps were generated from the horizons and used to create two-way-time (TWT) thickness and attribute maps. Attribute maps such as variance, root mean square (RMS), maximum amplitude, dip angle, dip azimuth and exact value were applied to image and investigate morphology of distinct features of interests such as mass-transport complexes, channels, regional and normal faults, pockmarks, furrows e.t.c observed in the area. Time slices and horizon mapping through the volume was useful for polygonal faults investigation. Iso-proportional slices were generated using a frequency decomposition volume in SVIPRO to image the deep-water channels in the eastern part of the study area (area 1). Bright spots for possible gas accumulation were defined from their anomalous high-amplitude reflections and reverse polarity produced as a result of presence of gas. Lithology is poorly constrained due to lack of well data.

OBSERVATIONS AND RESULTS

Sequence Stratigraphic Units

The studied interval encompasses the entire Cenozoic and Cretaceous successions bounded below by the Late Albian unconformity and top by the present-day seabed, which represents the post-transform interval (Figs. 2c, 4a-e). 3D seismic interpretation indicates presence of up to 2000 ms TWT (2 Km) thick post-transform interval assuming a velocity of 2 km/s (Fig. 4a-e). The tectono-stratigraphic framework of the interval is controlled by transform faulting that terminated in the Late Albian with deposition of thick post-transform sediments above the Top Albian unconformity above the faults (MacGregor *et al.,* 2003). Unconformity is represented by a strong positive amplitude reflection mapped only in the northern part due to limitation in the part of the data available data. The post-transform interval was divided into five (5) seismic units bounded by Six (6) surfaces traced from the Aje field and the use of seismic stratigraphic techniques is based on reflection terminations and seismic facies (Mitchum *et al.,* 1977). Units are described here as SU1 through to SU5 with the oldest being SU1 and youngest as SU5 (Figs. 4a-e, 5).

SU1 is characterized by transparent reflections and forms the entire Cretaceous section (Figs. 4). The unit is bounded at the top and base by the top Cretaceous and top Albian unconformities respectively (Fig. 2). Although no well data is available to determine lithology within the unit, but previous studies confirmed the unit is dominated by sandstone and shale (Brownfield & Charpentier 2006). The Late Cretaceous-aged sandstones form the reservoirs for the Aje and Seme fields and equivalent of the Jubilee field in Ghana (Fig. 2). Unit thickness reaches up to 800 ms along the western part but totally absent where the top Cretaceous unconformity merges with the top Albian unconformity (Fig. 5a). SU2 consists of variable reflections from low to high amplitudes. Reflections are very continuous and undulating especially in the centre (Fig. 4b). Occasionally, reflections are also very chaotic within the unit. Chaotic reflections are due to presence of mass transport deposits within the unit (Posamentier & Martinsen 2011). This unit encompasses Paleocene to Eocene-aged sediments, bounded above by a major unconformity (Eocene-Oligocene?). Sediment thickness within the unit reaches up to 1100 ms. TWT (Fig. 5b). Presence of thrust structures is observed within this unit (Fig. 4c).

The SU2 is overlained by the SU3 (Fig. 4). Internally, it is characterized by low to moderate amplitude reflections. Chaotic reflections are also prominent within the unit. It is bounded above and below by the Oligocene-Miocene and Eocene-Oligocene unconformities respectively (Fig. 2). The lower surface

erodes into the underlying unit (Fig. 4a). Thickness map of the unit reveals series of N-S oriented, elongated anticlines separated by alternating lows (Figs. 4b & 5c). Thickness reaches up to 700 ms TWT in the western part where large-scale deformed blocks were pushed down the slope (Fig. 5c). SU4 is characterised by very transparent, parallel reflections bounded at the base by the Oligocene-Miocene unconformity. The top was placed below overlying unit characterised by low to high-amplitude, reflections belonging to SU5 (Fig. 4).

SU4 is relatively thin in the centre of the study area (Fig. 5d). We interpreted the top of the SU4 as the base Pliocene interval based on change in seismic facies from underlying low-amplitude, transparent reflections to overlying low to high-amplitude reflections.

SU5 represents the youngest unit described in the study. It is characterised by low to high- amplitude reflections and often very chaotic (Fig. 4). The unit is bounded below and above by what we picked as the top of the Miocene section and seabed respectively. SU5 is dominantly characterised by mass transport deposits in area 2 (Figs. 6a, c & d). Area 1 within the unit is defined by series of high-amplitude, continuous to semi-continuous reflections associated with presence of deep-water channel complexes and fluid flow phenomena (Fig. 2). Structural framework of the basin is dominated by N-S elongated anticlines and NW-SE regional faults.

Seabed morphology

The morphology of the seabed in the study area is very irregular and imaged exceptionally in detail from time structure and attribute maps (Figs. 6 & 7). Dip angle and variance attribute on the seabed surface highlights key seabed features and provides an overview of related shallow, overburden features discussed in this paper. Both the seabed and sub-surface features are classified under depositional and fluid-flow products such as mass-transport deposits (MTDs), channels, sediment waves; and fluid flow elements include pockmarks, pipes, furrows, mound, bottom simulating reflector (BSRs) and polygonal faults. These features shape the seafloor bathymetry and would likely influence location of seafloor infrastructures. Structural highs and linear depressions created by faults were also well imaged (Fig. 6).

Area 1 is mainly characterized by seabed and overburden fluid flow features such as pockmarks, pipes, mound, furrows, BSRs and channels and some seafloor MTDs (Figs. 6 & 7). The headwall scarps and lateral margins of the MTDs are often well preserved on the seabed due to lack of subsequent deposition (Fig. 7) (Bull *et al.,* 2009). Two types of channels are observed on the seabed in this area and defined based on their level of sinuosity (Fig. 6). The main channel complex is highly sinuous and well imaged on the seabed maps (Figs. 6 & 7). A less sinuous channel is observed occur close to the end of the survey and the channel width increases down slope (Fig. 7). Both channels flow from NE-SW. Sediment wave train occurs west of the main channel and has a similar flow direction. The channels, MTDs and sediment wave train have similar flow direction (Fig. 7). Isolated pockmarks, although randomly distributed on the seafloor are associated with underlying structures. They are represented as circular to elongate depressions in plain view and on seismic section (Figs. 7a & c).

Area 2 is characterized by structural highs, MTDs and very straight and linear channels (Fig. 6). The channels and MTDs have a N-S and NW-SE flow direction respectively. Fluid-flow features were not observed on the seafloor within this area. Series of MTD blocks are observed on the seafloor in the

southwest corner of area 2 close to the end of the survey (Fig. 6). These blocks are up to 120 ms high and 150 m wide. These blocks are very protruding and form positive topography on the seabed, and internal reflections terminate against the upper wall of the block. Hummocky relief is observed on the seabed due to presence of near seabed mass transport complexes.

Understanding the distribution of these seabed features, which includes soft-sediment deformation, and fluid flow features, is useful, as they constitute geoharzards and should be evaluated before installation of offshore facilities. Presences of seabed and overburden fluid-flow features are possible indications of active petroleum system in the area 1.

Mass Transport Deposits (MTDs)

MTDs are important products of soft-sediment deformation in our basins in which very large volumes of sediments are transported down the slope during failure (Morscadelli & Wood, 2008; Bull *et al.,* 2009; Shipp *et al.,* 2011). They are often characterised by unique kinematic indicators well imaged from seismic data. Three main domains are commonly recognised in a mass-transport deposit. They are headwall, translational and toe domain (Fig. 7). Numerous and large-scale MTDs were identified vertically and laterally along the Nigeria Transform Margin and constitutes up to 50% of the entire stratigraphic section. This estimate may be low due to seismic resolution as smaller MTDs may be present. We adopt the general terminologies used by Bull *et al.,* (2009) to define these MTD's; these include headwall scarps, lateral margins, deformed blocks, pressure ridges, ramps and outrunner blocks (Shipp *et al.,* 2011 & references there in). Internally, MTDs are characterized by very low-amplitude, chaotic and discontinuous reflections (Posamentier & Kola, 2003; Posamentier & Martinsen, 2011); occasionally reflections could exhibit high-amplitude character as in sand-prone, submarine MTDs (Meckel, 2011).

Headwall domain

The headwall domain consists of the upslope region dominated mainly by extensional processes (Bull *et al.,* 2009). They include headwall scarps and extensional ridges and blocks (Fig. 7). The former is easily recognised from the seismic data both in seismic cross section and platform and represents the position of initiation of deformed unit (Figs. 8a & 9b). In cross sections, they are often observed as a normal fault displacement that separates the MTD from the un-deformed strata behind the headwall scarp (Fig. 9b). Series of headwall scarps ranging from few to tens of kilometres were identified in the area both on the seabed and from buried MTDs (Fig. 8a). The best-imaged ones are from the present-day seabed that have only recently occurred and no overburden deposition, although harder to see in seismic cross section (Fig. 8) (Martinez *et al.,* 2005; Bull *et al.,* 2009). The headwall scarp exhibits an actuate geometry and provides information on direction of movement of the sediments. In our case, sediments moved from northeast to southwest (Fig. 8a).

Translational domain

This region forms the main body of the MTD (Fig. 7). They are grouped under lateral margins (scarps; strike slip deformation), basal shear surface (ramps and flats; grooves and striations), internal body of

MTD (translated and outrunner blocks; slump folds) and top slide surface (longitudinal shears; secondary flow fabrics). Lateral margins are easily identified from the seabed MTDs (Fig. 7a). Lateral scarps/margins form the sides of the MTDs and parallel to slope direction processes (Bull *et al.,* 2009).

(It separates the undeformed strata from the deformed or failed strata (Fig. 9b). Lateral margins trend N-S suggesting overall flow direction in from northeast to southeast. A very important part of an MTC is the basal shear or detachment surface which underlies the entire failed unit or body (Zhu *et al.,* 2011). They are easily identified in seismic data and in outcrops (Posamentier & Martinsen 2011). N-S seismic section across the area shows at least 10 MTDs that lie on basal shear surfaces (Fig. 9a). They are often continuous but may be affected by ramps, faults, or other forms of displacements within the body of the MTD (Figs. 7, 9a & b). Ramps cuts down or upwards on the basal shear surface (Martinez *et al.,* 2005) and observed as a deep cut on the surface map (Fig. 9e). The most prominent ramps identified along the Nigeria Transform Margin occur on the base of SU5 and cut deeply into the SU4 (Figs. 9a & b). They vary in size, ranging from 3 Km to 20 Km and could be as deep as 150 ms TWT (Fig. 9a & e). Another major part of the MTD common in the area are translated and outrunner blocks (Figs. 7 & 9a-d).

Deformed blocks as high as 350 ms TWT and ~ 2 km in length are observed within SU 3 and 4 (Fig. 9a). They are similar in height to rafted blocks observed in Hinlopen Slide on the northern Svalbard Margin in the Arctic Ocean which are 450 m high and more than 5 km wide (Vanneste *et al.,* 2006). Reflections within the blocks, if preserved are rotated to near vertical and often chaotic. Individual blocks form pyramids, which tapers to the top with a flat or rugose base (Fig. 9a - c). They decrease in size down the slope (Fig. 9b) and surface mapped above the blocks reveals circular to oval-shaped, isolated features (Fig. 9c). Alternating depressions occur between the blocks and could form mini basins (Fig. 9c). Long, linear features often interpreted as glide tracks with outrunner blocks at the end are observed on the top surface map of the blocks (Figs. 9b) (Nissen *et al.,* 1999). A prominent eroded block is observed within SU5 (Figs.4b & 7). Internally, reflections are chaotic and transparent but surrounding reflections are characterised by high- amplitude, continuous reflections. It erodes into the underlying continuous, low amplitude unit SU4 (Fig. 7).

Toe domain

This represents the downslope part of a mass transport deposit, where it terminates or the region at which the movement stopped (Fig. 7) (Martinez *et al.,* 2005; Bull *et al.,* 2009). It is made up of compressional structures at the downslope of the MTD such as thrusts, folds, and pressure ridges (Fig. 7). Pressure ridges are semi-circular features associated with the end of a failed mass. Identifying these components of the MTDs helps to know what part of the system is being observed, and to make predictions the distribution of the MTD and its influence of other deep-water systems.

Utilizing combination of time surface maps and attribute extraction on the basal surfaces helped to investigate the presence and distribution of mass transport deposits. Based on this, we have mapped large-scale MTDs from seismic units 2 to 5 (Fig. 10). They are mostly concentrated in area 2. The amount of failed sediments that formed the MTDs also increases through time. Figure 10 highlights the MTDs mapped based on the basal surfaces from each one. In total, 22 mass transport deposits with varying sizes. Individual MTDs range from few kilometres to tens of kilometres in length and between 50 to 450 m thick. Individual volumes are not calculated but sizes should give an idea on the volumes of failed sediments along the slope during the Cenozoic. MTDs are not mapped in area 1 (Fig. 10). Seismic quality is very poor in within SU2 to SU4 in area 1 and often transparent. Locally where seismic is good, they are characterised by continuous reflections that are sometimes displaced by faults. SU5

in area 1 consists of entirely fluid flow features and deep-water channels (Fig. 6). Failed sediments are transported down the slope in the area.

Deep-water channels

Series of channels are observed along the Nigeria Transform Margin from 3D seismic data (Figs. 11 & 12) and generally form an important component of continental slopes. They include both active and buried channels and are well imaged on the seabed. Three main geometries are observed in the area based on the level of sinuosity.

Highly sinuous channels

These include highly sinuous channels active and paleo-channels (Fig. 11). The main channel complex (CC1) trends from northeast to southwest for about 20 km across the area. The full length both in up dip and down dip direction cannot be determined due to seismic data limit. It is highly sinuous and erosionally confined. Channels are represented as series of high-amplitude packages with strongly incised erosional bases (Fig. 11). Mapping of the channels in area 1 was important as they form an important part of the fluid flow history in the area. Iso-proportional slices from the seabed (t10) to the base of the high-amplitude, reflection package (t1) revealed the channel geometry and other buried channels (Fig. 11). The slices show the evolution of the channels through time. Five channel complexes are revealed. CC1 and CC5 are active channels while CC2- CC4 are paleo-channels. Lithology within the channels cannot be ascertained without well data but based on high-amplitude character; channels are likely to be sandstone-rich. CC1 becomes more confined with time and occur in close relation with sediment waves (time 10). CSS5 is less sinuous and looks more like a levee of another channel but its location at the end of the survey makes it challenging to confirm this (Fig. 6). Circular depressions are observed along channel margin and within channel axis of both active and buried channel complexes.

Linear channels

Series of depressions are observed on the seafloor within areas 2 and 3 (Figs. 5 & 12). Seismic profiles show the depressions are only between 10 – 15 m deep and up to 250 m wide (Fig. 12). Time structure map and attribute extraction on the seafloor reveals that depressions are often continuous and forms linear and narrow features, which are clearly seen on the seabed (Figs. 11a, d & h). The long and linear features are only observed within areas 2 and 3 and have N-S and NE-SW orientation respectively. They are interpreted as linear channels with no sinuosity similar to those observed offshore Angola (Gee & Gawthorpe 2007). According to them, they suggested the linear channels were formed from erosional lineation on the slope created by large and infrequent turbidity current and often affected by complex topography. Azimuth map of the seabed in the study area shows how these linear channels are deflected around the structural high and MTD blocks such that channels are compressed close to the structures and then bifurcates forming newer channels (Fig. 12a&b). We describe 3 phases, which includes the normal phase, where channels have not been affected by structural high or MTD blocks. Seismic profile c shows only 3 channels (1 – 3) (Fig. 12c), but close to the structural high the channels are compressed and deflected by the high, which represents the second phase. Finally, the bifurcation phase where channels 1 and 2 bifurcates and forms additional channels 5 and 4 respectively (Figs. 12). Width of individual channel also decreases towards the structural high. Based on this we support earlier

interpretations from offshore Angola by Gee & Gawthorpe (2007), that these linear channels are affected by complex topography

Sediment waves

RMS attribute at -50 ms below the seabed reveals a 25 km long linear feature in the eastern part of the study area (Fig. 13a). Average width across the feature is 2 km, which increases abruptly in the southern part and forms a lobe similar to terminal lobes within deep-water environments. It has the same NE-SW orientation as the main channel system but terminates before the end of the survey. The attribute map shows that the bright amplitudes imaged within the feature correlates to high-amplitude, anomalous reflections on seismic cross section across the feature (Fig. 13b). Seismic profile through the lobate part of the feature shows the anomalies are constrained with looks like a cut-off loop of the channel and interpreted as a sediment-wave train (Fig. 13c).

This pattern of sediment waves developed within what could have been an abandoned channel, hence the shape (Fig. 13a). The down-dip lobate part of the sediment wave could have represented the cut-off loop of the old channel (Fig. 13a & c). We assume the sediment waves were formed by turbidity current. Sediment waves within leveed channel complex and channel overbank have been interpreted in the Niger Delta basin (Posamentier & Kolla 2003; Sutton & Mitchum, 2011). Relationship of sediment waves observed in the area with gravity-induced processes suggests they were created by turbidity currents.

Fluid Flow Phenomena

Pipes and high-amplitude reflections

Vertical and narrow columns in form of pipes are clearly visible from seismic cross section in the upper stratigraphic seismic unit 5 of the study area. They are between 50 – 80 m wide and extend about 400 ms below the seabed (Fig. 14a). Within the features, seismic response is slightly distorted, and reflections are either concave downwards inform of stacked intervals of pull-up structures or concave upwards inform of stacked cones (Figs. 14c-g). Surrounding reflections are normal and continuous. They are often located below seabed depressions and have a circular to oval shape on time slice (inset of fig. 14a). In the northern part of area 1, these vertical columns terminate above a structural high at about 2150 ms TWT below the present day seabed. Similar features have been interpreted as blow-out pipes formed because of fluid migration through the stratigraphic succession (Løseth *et al.,* 2001; 2011; Gay *et al.,* 2007; Cartwright *et al.,* 2007; Moss & Cartwright 2010; Huuse *et al.,* 2010). In the study area, the structural high is faulted at the crest by series of normal faults (Fig. 14a). Amplitude quality diminishes with the vertical columns and increase towards the top of the structural high. Amplitude anomalies are often observed either directly below the column (Fig. 14d) or adjacent to it at the level at which the columns terminate (Fig. 14a & f). In most cases, the high-amplitude reflections are characterized by high-amplitude, reflection packages with reversed seabed polarity, such that a hard kick is overlain by a soft kick (Fig. 13a) (Schroot & Schuttenhelm, 2003; Andreassen *et al.,* 2007). These amplitude anomalies form bright spots and could be associated with gas accumulation. Occasionally, the bright spots also terminate against the fault plane (Fig. 14f). Similar bright amplitude or bright spots beneath or along vertical zones have also described in other parts of the deep-water Niger Delta basin (Loseth *et al.,* 2001; 2011) and Barent Sea (Andreassen *et al.,* 2007). They are often interpreted to be associated with gas accumulations such as gas charged sands within deep-marine reservoir channels or fans. Based on the observations presented above, the vertical columns are interpreted as pipes. These pipes as well as faults can act as

pathways for underlying fluids to migrate and be expelled onto paleo or present day seafloor (Gay *et al.,* 2004; Ligtenberg 2005; Loseth *et al.,* 2009; Ho *et al.,* 2012).

Pockmarks

Numerous depressions are identified on the seabed from seismic cross section (Fig. 14a). They exhibit circular, oval, or elongate geometries in plain view and are randomly distributed (Fig. 14b). These depressions have been observed both on the present-day seabed and paleo seabed. They are interpreted as pockmarks (Hovland & Judd 1988; Heggeland 1998; Judd & Hovland 2007; Gay *et al.,* 2006a, 2006b). Since their first recognition on the Scotian shelf from sidescan records by King & MacLean (1970), these fluid flow features have been documented in several basins in the world (Rise et al., 1999; Ligtenberg 2005; Judd & Hovland 2007; Gay *et al.,* 2007; Andresen, 2012; Reiche *et al.,* 2011; Ostanin *et al.,* 2012). Original simple geometries of pockmarks can be altered through merging of individual pockmarks, carbonate precipitation and bottom current erosion to produce more diverse range of geometries such as elongated, bulls-eye, composite and complex (Andresen *et al.,* 2008). Pockmarks identified along the Nigeria Transform Margin are classified based on geometry, occurrence and location and are observed within area 1 (Fig. 6).

Isolated/Scattered and pipe-related pockmarks

In seismic cross sections, they are observed as V or U-shaped depressions on the present day seabed. They are up to 15 ms deep and up to 60 m wide, isolated depressions and scattered randomly on the seabed above a structural high in the northern part of area 1 (Fig. 14). Spacing between individual pockmarks is irregular and they occur directly above underlying vertical columns interpreted as pipes (Fig. 14a). The isolated pockmarks and vertical pipes are likely to be genetically related. Relationship between pockmarks, pipes and sandstone reservoir was identified in the deep-water Niger Delta (Loseth *et al.,* 2001; 2011). It was suggested that crater-like depressions on the seabed formed from gas expulsion from underlying hydrocarbon-charged reservoir unit.

Stacked pockmarks

Five horizons were interpreted locally around what appears to be vertically, stacked depressions between 1975 – 2275 ms TWT in the eastern part of the study area (Fig. 15a). In plain view, depressions exhibit circular geometry on each of the horizons (Fig. 15b). Depth of individual depression and width varies between 10 – 35 ms and 270 – 480 m from shoulder to shoulder respectively (Fig. 15b). Depth and width of the stacked pockmarks increases with depth (Figs. 15bi-iv). This relationship changes on the last horizon mapped (Fig. 15bv). It is unclear as to what is controlling the change in dimensions, but we observe the deepest depression also coincides with presence of an increase in amplitude (Fig. 15a). The stacked depressions are associated with the hanging wall of the faults and the high-amplitude, soft-kick reflections (possible gas accumulation) terminate against the fault plane (Fig. 15a & d). They are interpreted as stacked pockmarks similar to those from the Lower Congo Basin and other sedimentary basins and indicative of repeated fluid expulsion within the sedimentary column (Cartwright *et al.,* 2007; Andresen & Huuse 2008; Martinez *et al.,* 2011).

Fault-related pockmarks

Circular or elongated depressions observed with normal faults along the Nigeria Transform Margin are interpreted as pockmarks (Fig. 15a-e) (Hovland & Judd, 1988). The seismic profile and attribute maps below the seabed show presence of pockmarks along and above faults (Fig. 15e & f). The faults are oriented NW-SE, perpendicular to the channels and MTDs on the seabed (Fig. 6). Occasionally, the faults offset the present day seabed and create linear depressions on the seafloor (Fig. 15f). This suggests faults are likely active. These pockmarks occur either along the hanging wall of the faults (Fig. 15d) or directly above fault planes (Fig. 15e) as in fault-hanging wall and fault-strike pockmarks respectively similar to those observed in other parts of the West African margin (Pilcher & Argent, 2007). Presence of pockmarks along faults is likely indication of fluid leakage through the fault (Ligtenberg, 2005). Pockmark and fault relation is well documented from the Lower Congo Basin; the faults create curved depression on the sea floor and served as pathways for fluid migration (Gay et al., 2007).

Channel-related pockmarks

Variance attribute extracted on the seabed shows large number of depressions (red arrows) similar in size and depth as those described above within the channel axis and along margins of both active and buried channel complexes and interpreted as pockmarks (Fig. 16) (Hovland & Judd 1988). These pockmarks are 200 – 300 m wide and depth of ~ 50 ms TWT. They are mostly circular in plain view and more regularly spaced about 1km than those observed above the structural high (Fig. 14b). The pockmarks follow the meandering geometry of the channels (Fig. 15). The paleo-channels are located at about 200 – 250 ms below the seabed where the pockmarks occur (Figs. 16d & e). The channels are characterised by high-amplitude reflections suggesting sandstone lithology. Presence of pockmarks above stacked turbiditic paleo-channels has been well documented in the Lower Congo basin (Gay *et al.,* 2003, 2004, 2006, 2007). Pockmark formations have been attributed to fluid expulsion from these active and buried channels with the fluids sourced either directly from the channels or from deeper intervals and the channels acted as permeable conduits for fluid migration (Gay *et al.,* 2006, 2007). Variance attribute on the seabed shows presence of small faults above buried channels, these faults could have enhanced upward fluid migration from underlying buried channels forming pockmarks on the present day seabed (Fig. 16a). Fluid expulsion from deep-water channels has also been associated with emplacement of sandstone injectite in the deep-water Niger delta towards the eastern part of the study area (Davies, 2003).

Elongated pockmarks

Series of high-amplitude, wedge-shaped anomalies are observed at ~ 25 ms below the seabed (Fig. 17). These anomalies are characterized by two full reflection cycles starting with a hard-kick at the top and a soft kick at the base. They are isolated packages, about 25 ms thick and terminate against fault planes (Fig. 17b). Thickness of each reflection package increases towards the fault plane and wedges away from it. Amplitude diminishes away from the fault plane into continuous reflection like surrounding strata (Fig. 17a, b & d). The high-amplitude packages are layer-bound and occur continuously for about 15 km. RMS attribute extracted on the yellow horizon located

~100 ms below the seabed with a window length of 75 ms revealed the plan view geometry and distribution of these wedge-shaped, high-amplitude anomalies (Fig. 17a & c). The map reveals several randomly spaced, circular-oval or elongated shaped depressions oriented in NW-SE or W- E direction (Fig. 17a). Based on their geometries, they are interpreted as circular pockmarks and elongated pockmarks respectively. These elongated pockmarks are up to 1500 m long and 200 m wide. Similar features have been interpreted as furrows along the mid-Norwegian margin (Reiche *et al.,* 2011) and Lower Congo basin (Gay *et al.,* 2004); they are related to normal faults.

We observe a unique relation between underlying normal faults, high-amplitude, wedge-shaped features, and furrows (Fig. 17). Where underlying regional faults propagate through shallower sediments and wedge-shaped anomalies terminate against the fault plane, elongated pockmarks are formed in contrast to normal circular pockmarks formed where such relationship is not defined. This is clearly observed in furrows number 7, 8 and 9 as opposed to pockmarks 3 and 4 (Fig. 17).

This relationship could also suggest a transition from individual circular to elongated pockmarks created due to subsequent remodification of the pockmark geometry by deep-seated faults (inset in Fig. 17d). Suggesting they could have been formed initially as circular depressions but remodified by faulting to create present elongate or linear geometries. Similar transition model from circular pockmarks to elongated pockmarks (furrows) was proposed in the central North Sea and elongation was attributed to bottom current (Kilhams *et al.,* 2011). The interval at which high- amplitude, wedge-shaped feature occur is highly faulted with smaller extensional faults (Fig. 17). Some of the planes of these faults coincide with the regional faults, and as such associated with the pockmarks.

Gas-Hydrate Bottom Simulating Reflector (BSR)

The seismic cross section shows the presence of a continuous reflection with negative polarity at about 300 ms below the seabed within SU5 (Fig. 18). The reflection tracks the seabed reflection but exhibit a cross cutting relationship with surrounding stratigraphic reflections (Fig. 18c). The reflection is consistently located at the same depth below the present day seabed (Fig. 18a). Below the reflection are series of high-amplitude packages with reverse seabed polarity. These packages have been interpreted as free gas accumulations. Based on geometry, reflection character, depth below the seabed and location of possible gas accumulation in the underlying interval, the reflection is interpreted as a bottom simulating reflector (BSR) (Shipley *et al.,* 1979). BSRs are often observed in deep-water settings and associated with low temperature and high pressure (Shipley *et al.,* 1979). They are primarily associated with gas hydrates and represent the bottom of a gas hydrate stability zone GHSZ (Gay *et al.,* 2007; Serie *et al.,* 2012). The negative acoustic response is formed from contrast between over lying; high-velocity gas hydrate zone and underlying; low-velocity free gas-saturated sediments (Gay *et al.,* 2003; Berndt *et al.,* 2004). Numerous gas hydrates have been documented on the continental in Nigeria down to southern Angola (Cunningham & Lindholm, 2000). Their occurrence with channels, faults and mobile substrate structures have also been documented along these margins.

The BSR was mapped only where cross cutting relationship is observed. It is locally present and restricted to area 1 as with other fluid flow features described in previous sections. A relationship is observed between BSR occurrence and faults in the study area such that the mapped limit of the BSR correlates to location of regional faults in the area suggesting a genetic relationship (Fig. 18c). Some of the deep-seated faults terminate below the gas hydrate stability zone while others propagate further into the shallower section (Fig. 18a & b). Extent of the BSR mapped in the area suggests extent of gas hydrates present within the SU5, although this could have been underestimated or overestimated as previous drilling through BSR have not penetrated any gas hydrates and gas hydrates have also been encountered without evidence of BSR (Hovland, 2005). Pockmarks are observed on the present day seabed above gas hydrates (Fig. 18e & d). Previously, presence of gas hydrates and BSR was thought to impede upward flow of fluid through the gas hydrate stability zone but continuous identification of fluid flow phenomena such as pockmarks, pipes, gas hydrate pingoes above BSRs suggests otherwise (Cummingham & Lindolm 2000; Hovland 2005; Gay *et al.,* 2006a; Ostanin *et al.,* 2012; Serie *et al.,* 2012). The interval above BSR is faulted by small extensional faults and these faults could have permitted migration of gas through the

sedimentary column to the seabed as pockmarks. Hydrate dissolution have also been proposed as a potential mechanism for pockmark formation in the Niger Delta due to excessive overpressure generated during dissolution process (Sultan *et al.,* 2010).

Seafloor Mound

In the south-eastern part of the study within area 1, a 30 ms high and 500 m wide positive feature is observed on the seabed (Fig. 19). This is well imaged from the attribute maps and frequency decomposition map of the seabed as an isolated dome-shaped structure in form of a mound (Figs. 6 & 11). At about 20 ms TWT below, there is a marked increase in amplitude in the reflection followed by a soft reflection event (Fig. 19b & c). Below the high-amplitude zone is a cylindrical- shaped, vertical feature well imaged on the seismic cross section and characterised by very low to transparent or distorted amplitudes. The cylindrical-shaped feature is ~ 300 ms long between 2425 and 2725 ms with different reflection character from surrounding strata. Internally, reflections form series of stacked pull-up geometries about 20 ms high suggestive of a high-velocity mound fill. Using a background velocity of 2 km/s, the velocity within the mound was estimated as ~ 3.3 km/s.

Although surrounding reflections can be traced within the vertical column, but reflection are very weak with variable continuity. The transition between the surrounding strata and vertical column is abrupt and clearly imaged in cross section (Fig. 19b). In time slice, the feature forms a circular geometry and is located about 5km close to the main channel complex. Gay *et al.,* (2007) described a similar feature on the seabed from Lower Congo Basin and core analysis suggested carbonate-rich sediments with cold-water corals interbedded with hemipelagic muds. A single mound was also described on the mid- Miocene unconformity that represented a paleo-seabed in the Norwegian-Danish basin and Northern North Sea; they were interpreted as sand extrudite (Andresen e*t al.,* 2009; Olobayo *et al.,* 2015b). Other possible origins for the dome-shaped or circular feature on the seabed or in the sub-surface are mud volcano, shale diapir, salt body, carbonate mound, (Stewart 1999). No well or core information is available in the area to ascertain the lithology within the mound. A salt origin is discarded, as there is no evidence of halokensis in the area. Seismic amplitude character below the mound is similar to those described from the Angola Margin as gas hydrate pingoes (Serie *et al.,* 2012).

The vertical column is rooted within high-amplitude, semi-continuous to discontinuous reflection packages interpreted as sandstone-rich channel (Fig. 19b & c). Opacity rendering was applied on a cropped volume to show relationship between the seabed mound, vertical column, and underlying sandstone-rich channel (Fig. 19d). Time slices through the vertical column below the mound shows circular geometry of the column and a neighbouring pockmark (Fig. 19e). Mound volcanoes have been described from the Niger-Delta basin but location of mound above a possible sandstone-rich channel makes a mound lithology unlikely (Graue 2000). However, due to the very high velocity within the mound (~3.3 km/s) a sandstone origin is also unlikely. Lithologies known to produce such high seismic velocities are often carbonates (Anselmetti & Eberli, 2012). We therefore propose a methane-derived carbonate mound origin formed from fluid sourced from underlying channel sands through the vertical column (Fig. 16d & e) (Cauquil & Adamy 2008, OTC).

Polygonal Faults

The seismic data reveal presence of networks of small, extensional normal faults in the area (Fig. 20). These faults are well imaged in the first 400 ms TWT below the seabed (Fig. 20 a & c). Fault throws measured are less than 12 m (between 3 – 11 m, 6 m average) and dip angle range of 41 – 50º (46º

average) assuming a velocity of using 2000 m/s (Tab. 2). Time structure map, original amplitude, and variance attribute extraction on horizons through the highly faulted succession shows faults form polygonal geometry in plain view (Fig. 20 b & d). Similar faults have been interpreted as polygonal faults, which was first recognised within Eocene succession of the North Sea basin and defined as layer-bound faults formed from dewatering of fine-grained sediments particularly mudstones during early burial (Cartwright 1994; Lonergan & Cartwright, 1999; Lonergan *et al.,* 1998; Goulty 2001; Stuevold *et al*., 2003). They have since then been interpreted in several basins in the world within mainly fine-grained mudstones (Appendix 1.1). Other mechanisms recognised to cause shear failure in fine-grained sediments and attributed to their formation include gravity loading, alteration of volcanic ash, silica diagenetic reactions (Cartwright, 2011).

Based on observations above, we interpret these faults as polygonal faults, and this study presents the first-ever documentation of polygonal faults in the deep-water settings of Nigeria. These polygonal faults have similar dip angles with those recorded in the North Sea and Faroe-Shetland but smaller fault throws (Tab. 2). They deform the SU3 - SU5 and occur in two tiers separated by a non-polygonally faulted interval; the upper tier tip terminates about 50 ms below the seabed and better imaged than the lower tier in SU3. The polygonal faults are randomly oriented in most parts the study area but close to the regional faults, the faults become linear and preferentially aligned with the NE-SW regional faults but perpendicular to the NW-SE regional faults (Fig. 20b & d).

The presence of polygonal faults within Pliocene to Holocene sediments suggests they are still fairly recent and could explain why they have very small throws compared to those documented in the North Sea and Faroe-Shetland basins formed within much older sediments and terminate at the mid-Miocene and Intra-Oligocene unconformities respectively (Lonergan *et al.,* 1998; Shoulders *et al.,* 2007; Olobayo *et al.,* 2015; Chapters 3-5). In the Lower Congo basin, similar faults are documented within Pliocene-aged sediments below the seabed and have similar throws as those observed along the Nigeria Transform Margin (Tab. 2). Another characteristic feature observed between the faults along both margins is occurrence of alternating layers with low and high- amplitude anomalies through the faulted interval (Gay *et al.,* 2004). Where this is observed in the study area, the polygonal faults are more visible in seismic cross sections, and this could be related to lithological characteristics. Polygonal faults observed along the Nigeria Transform Margin are more extensive than other fluid flow features and present within areas 1 and 2 (Figs. 4b-d & 20). Their occurrence along the margin and in the south within the Lower Congo basin and similarity in characteristics could suggest regional occurrence of these layer-bounded faults along the entire margin.

DISCUSSION

This section summarizes the mechanism of MTD formation, controls on fluid flow distribution and fluid source. A summary diagram highlights all the deep-water depositional elements and fluid flow phenomena interpreted in the study area (Fig. 21).

Mechanism of MTD formation

Mass transport deposits can be recognised at a variety of scales ranging from small-scale as in cores, medium-scale in outcrop and to regional seismic scales such as the Storegga slide offshore Norway (Bull *et al.,* 2009; Shipp *et al.,* 2011; Dykstra *et al.,* 2014). Regardless of the scale at which they occur, MTDs are direct response to slope instability in sedimentary basins (Posamentier & Martinsen 2011). We presented in the previous section, multi-event MTDs from the Nigeria Transform Margin. They include

both buried and active MTDs from SU2 to present day suggesting repeated slope failure throughout the Cenozoic (Fig. 10). We also observed the magnitude of failed sediment increased through time in the area (Fig. 10). These mass transport complexes occur in association with other deep-water deposition elements such as channels and sediment waves (Fig. 6). Based on our observations presented in previous sections, the MTDs occur primarily within area 2 and described as the mass transport deposit zone (Fig. 22a).

Numerous studies have documented several mechanisms that cause slope failure, some of which includes slope instability, conversion of Opal A to CT, gas-hydrate destabilization, gas release, earthquake shaking, sea level changes, rapid or increased sedimentation, slope gradient (Davies & Clark 2006; Garziglia *et al.,* 2008; Zhu *et al.,* 2011; Nelson *et al.,* 2011). This product of soft-sediment remobilization or deformation is primarily triggered by difference in pore pressure within the sediment (Martinez *et al.,* 2011).

We investigated some of these mechanisms in our study area and discuss them below. Silica diagenetic transformation of opal A to opal CT has been proposed previously as a trigger for submarine failure in the Faroe-Shetland basin (Davies & Clark 2006). Due to elevated pore pressure during conversion of opal A to CT can result rapid compaction and reduction in sediment shear strength making it susceptible to failure. This however is unlikely in our area, as we do not have any evidence of opal A to opal CT transformation.

A bottom simulating reflector was interpreted locally as the contact between gas hydrate bearing sediments and sediments hosting free gas within SU5 (Pliocene- recent) sediments in area 1, which is also where fluid flow phenomena dominate. In contrast, MTDs in SU2-5 occur more regionally in area 2 where no evidence of thermogenic fluid is observed. However, we do not discount the possibility of formation water release from consolidation of sediment (Van Rensbergen *et al.,* 2003).

An alternative and common mechanism for formation of episodic mass transport deposit is sea level change (Nelson *et al.,* 2011). We have no absolute ages for the MTDs in the area to be able to match to sea level rise and fall making it difficult to relate the MTD sheets to sea level rise and fall. However, there was significant global fall in sea level at the onset of the Pliocene (Fig. 2). This correlates to the period of major increase of MTD development in our study area (Fig. 10). Even though, this alone is not sufficient to make reasonable conclusions, we cannot rule out the effect of sea level on episodic MTD formation as we do not have enough information for this.

We considered effect of tectonics and earthquake activities. Nigeria Transform Margin falls within the Equatorial conjugate margin characterized by complex wrench and transform faulting. However, transform tectonism was active until Middle to Late Albian time, marked by development of the Late Albian unconformity (Brownfield & Charpentier 2006). This unconformity represents the lower bounding surface of our interval of study, suggesting transform tectonism was no longer active, but continuous extension of the crust resulted increase clastic deposition and thermal subsidence which continued till the Tertiary period in the area (Brownfield & Charpentier 2006).

Net sediment accumulation rate from the Late Albian unconformity to present day seabed was estimated using a simple calculation method adopted from Jordt *et al.,* (2000) (Tab. 3) and a representative graph was plotted (Fig. 23). TWT values were obtained from thickness maps and a constant velocity of 2 km/s was used. It should be noted that results do not account for compaction, burial or erosion and only based on estimates given the data available.

Table 3 and Figure 23 show increased sedimentation through time which corresponds to increase in magnitude of MTDs formed (Fig. 10). Decrease in rate of sedimentation between SU3 and SU4 can also be observed from the distribution map of the MTDs. Significant increase from 39.5 m/Ma in SU4 to 150.9 m/Ma in SU5 is also reflected from the MTD map. Based on this, we suggest formation of episodic MTD on the Nigeria Transform Margin was mainly driven rate of sedimentation and increase in magnitude of failed sediment was also controlled by sedimentation.

Over steepening of the slope could also be a contributing factor to slope failure in the area. Slope gradient measured is ~ 1° for the present day and this could have enhanced rapid deposition or slope progradation of sediments especially in an area with high sedimentation rate (Zhu *et al.,* 2011).

Controls on fluid flow features and distribution

Interpretation of 3D seismic data from the Nigeria Transform Margin shows evidence of fluid-flow features within SU5 in area 1 (Fig. 6, 21 & 22). Lack of other data such as well data, geochemical data or seepage slick from area makes interpretation based solely on observations made from the seismic data and previous studies. Analysis of these features was carried out using volume and surface attribute extractions to reveal their geometries and spatial distribution along the margin. A summary table of all the fluid flow products interpreted in the area is shown in figure 20. These include pockmarks, pipes, BSR, furrows seafloor mounds and polygonal faults (Fig. 20). They occur both on the present day seabed and below the seabed.

Pockmarks are attributed to upward expulsion of fluids either gas or water from an underlying source, they give indication of the presence of an active petroleum system (Hovland & Judd 1988, Rise *et al.,* 1999; Gay *et al.,* 2007; Judd & Hovland 2007) and are classified as focused fluid flow features alongside with chimneys, pipes, and sandstone intrusions (Cartwright 2007; Huuse *et al.,* 2010). Although pockmarks are randomly distributed, they are related to structural highs, deep- seated, regional faults and active and buried deep-water channels (Figs. 14-17). These erosional and tectonic structures constitute an important component of the plumbing system in the area (Fig. 22). Based on observations and interpretations from the area, we suggest these features have served as migration pathways either through focused zones of weaknesses along the faults or diffused within permeable sediments as in sandstone-rich channels (Ligtenberg 2005; Pilcher & Argent 2007; Gay *et al., 2006,* 2007). Active petroleum plays exist along the West Africa Transform Margin, which includes the syn-transform Aptian-Albian fields such as Hihon, Fifa, Tano and the younger, post-transform Upper Cretaceous fields such as Aje, Panthere, Belier sourced from Cretaceous shales (Greenhalgh *et al.,* 2011). Most of the regional faults in area 1 are deep-seated and goes down into the Cretaceous interval where source and reservoir rocks within the basin are located (Fig. 2b). Pockmarks, pipes, furrows and BSR are related to faults (Figs. 22b, c, g-i) while the mound and pockmarks are related to active and buried channels (Figs. 22d-f). Seismic quality below the channels is very poor and chaotic, which made it difficult to map regional faults below the channel complexes (Fig. 4e). It is therefore assumed that fluids that generated pockmarks above the channels could either have been sourced from within the channels or through faults if present (Figs. 22d-f).

Fluid type, source and driving mechanism

Lack of geochemical data made it difficult to ascertain the type of fluid expelled during the formation of these seabed and overburden fluid flow features. Most likely fluids are water, gas, or oil. In the Lower Congo basin, core samples were taken from pockmarks for geochemical analysis, and this confirmed the presence of biogenic gas, thermogenic gas and combination of the two (Gay et al., 2006a). Presence of

bright spots with reverse seabed polarity along fault planes and below pipes, and possible free gas below BSR strongly suggests presence of gas in the area (Figs. 14 & 22b, d & g-i). The Aje field located in OML113 in the northern part of the area is a successful gas field with its reservoirs within the Cretaceous interval (Fig. 1b & 2c). Recent drilling into Cretaceous sandstones in OPL310 (Ogo discovery) east of Aje field to the north of the study area also encountered significant accumulation of oil, supporting the notion of an active petroleum system in the area.

Based on this, we suggest that fluid type is likely to be either gas or oil. However, we cannot exclude that pore water expelled from reservoirs also contributed to it because of differential compaction of coarse-grained sediments and fine-grained mudstones. Regional faults, which are rooted within Cretaceous interval, occur in association with fluid flow phenomena and likely to have facilitated upward migration of fluid from deeper intervals. It is unclear whether the faults are sealing or not but presence of fluid flow features or seal bypass systems in the shallow interval could suggest leakage along faults (Cartwright *et al.,* 2007). We support both biogenic origin of hydrocarbon from shallow interval and thermogenic origin from deeper reservoirs or combination of both for hydrocarbon source. However, this cannot be confirmed without appropriate geochemical analysis (Judd & Hovland 2007).

In the study area, all the fluid flow products occur with the shallow Pliocene to recent section (SU5) (Fig. 22b-i). This coincides with timing of hydrocarbon generation and migration in the Cretaceous source rocks within the Dahomey-Benin basin, which started in the Late Miocene and continued till date, although much earlier in other basins along the transform margin (Brownfield & Charpentier 2006). Based on this, we suggest timing of fluid flow products formation began after Late Miocene till the present day and fluid flow was triggered as a result of hydrocarbon generation within the basin. This assumption also supports a thermogenic origin for fluids in the area.

Implications

Presence of mass transport deposits and fluid-flow features are geological hazards as they result in slope instability and should be investigated before placement of drilling infrastructures (Shipp *et al.,* 2011). MTDs constitute a significant portion of the entire succession and could have impact on sediment pathways and distribution. They can also serve as seals and reservoirs of source rock under the right conditions (Posamentier & Martinsen 2011). Episodic development of MTDs that are related to sea level falls have important implications for hydrocarbon reservoir studies as failed sediments could have been pushed down the slope or basin along with turbidites which are important targets for hydrocarbon exploration (Nelson *et al.,* 2011).

Pockmarks, pipes and BSRs are evidence of active petroleum systems if formed from hydrocarbon but however, their presence also suggests breach in sealing sequence as in sandstone intrusions in the North Sea (Cartwright *et al.,* 2009; Huuse & Cartwright 2007; Olobayo *et al.,* 2015; Chapter 4). Impacts of pockmarks and other seabed fluid flow features on geology, biology and marine environment has been well documented by Judd & Hovland (2007). According to Cauquil and Adamy (OTC 2008), pockmarks and other seabed depressions are considered geoharzards during deep-water exploration and production activities and must be identified and evaluated at the early stages of the project. They went ahead to say that these seabed depressions may affect subsea installations and must be mapped out carefully before installations of drilling equipment on the seabed (Martinez *et al.,* 2011).

CONCLUSIONS

Based on analysis of 3D seismic data available; we divided the post-transform succession into five

(5) major seismic units bounded by significant surfaces and major unconformities to investigate depositional and fluid-flow elements along the Nigeria Transform Margin. Conclusions from this study are:

- Presence of depositional, soft-sediment remobilization/deformation and numerous fluid- flow features, which shaped the seafloor topography and overburden succession have been identified on the Nigeria Transform Margin.
- Spatial and temporal occurrence of repeated, large-scale, mass transport deposits along the margin through time is indicative of long-term of slope instability and forms up to 40% of the stratigraphic section within area 2.
- Increased sedimentation has been proposed as major mechanism for repeated mass transport deposit in the area. Slope gradient and sea level change could also have contributed.
- The continental slope is deeply incised in eastern part by well-developed, meandering deep-water channels and gently incised by linear and elongated channels in the centre and western part of the area as revealed from the seabed topography map.
- Occurrence of fluid-flow features such as pockmarks, pipes, furrows, methane-derived carbonate mound and bottom simulating reflection are restricted to area 1. This suggests presence of active petroleum system in the area as well as indication of seal leakage.
- Relationship between pockmarks, pipes, furrows, and bottom simulating reflection with regional, deep-seated faults suggests faults could have acted as migration pathways for upward fluid migration from underlying reservoirs.
- Three (3) main fluid sources are suggested; they include pore water, hydrocarbon from biogenic and thermogenic origin. This can only be confirmed with additional data such as geochemical data.
- Hydrocarbon generation and expulsion was proposed as the driving mechanism for formation of fluid flow features in the area.
- First documentation of polygonal faults within the western part of Nigeria margin. These faults have similar dip angles, but smaller throw compared to polygonal faults in the North Sea and Faroe-Shetland basins. Fault throws are similar to those interpreted from the Lower Congo basin
- Results from this study will be useful during exploration and production as mass transport deposits and fluid flow features could form potential geohazards and their distribution should be mapped out and evaluated at the onset of exploration.

ACKNOWLEDGEMENTS

We wish to thank Petroleum Technology Development Fund (PTDF) Nigeria for proving full scholarship that has made this research possible. We want to thank PGS for providing the 3D seismic

volume for this project. Appreciation also goes to the editor and reviewers for their constructive comments in the process of reviewing this paper.

REFERENCES

ANDRESEN, K.J., CLAUSEN, O.R., HUUSE, M. (2009). A giant (5.3×107 m3) middle Miocene (c. 15 Ma) sediment mound (M1) above the Siri Canyon, Norwegian–Danish Basin: origin and significance. Marine and Petroleum Geology 26, 1640–1655.

ANDRESEN, K.J., HUUSE, M. & CLAUSEN, O.R. (2008). Morphology and distribution of Oligocene and Miocene pockmarks in the Danish North Sea – implications for bottom current activity and fluid migration. *Basin Research,* 20, 445–46.

ANDREASSEN , K., NILSSEN, E.G. & ØDEGAARD, C.M (2007). Analysis of shallow gas and fluid migration within the Plio-Pleistocene sedimentary succession of the SW Barents Sea continental margin using 3D seismic data. *Geo-Marine letter, 27*, 155 – 171.

ANDRESEN, K. J (2012). Fluid flow features in hydrocarbon plumbing systems: What do they tell us about the basin evolution? *Marine and Petroleum Geology, 26*, 1640-1655.

ANSELMETTI, F.S. & EBERLI, G.P (2012). Controls on sonic velocity in carbonates. *Pure and Applied Geophysics, 141,* 287-323.

BERNDT, C., BÜNZ, S., CLAYTON, T., MIENERT, J., SAUNDERS, M., (2004). Seismic character of bottom simulating reflectors: examples from the mid-Norwegian margin. *Marine and Petroleum Geology 21,* 723–733.

BLAREZ, E., & MASCLE, J. (1988). Shallow structures and evolution of the Ivory Coast and Ghana transform margin*: Marine and Petroleum Geology, 5*, 54–64.

BORSATO, R., GREENHALGH, J., MARTIN, M., ZIEGLER, T., MARKWICK, P & QUALLINGTON, A. (2012). Atlantic Conjugate Margin: an exploration strategy. PGS presentation in London.

BORSATO, R., GREENHALGH, J., WELLS, S., ROBERSON, R., & FONTES, C. (?) Prospectivity of the Equatorial Conjugate Margins of Africa and South America: PGS presentation.

BROWNFIELD, M.E., and CHARPENTIER, R. (2006). Geology and total petroleum systems of the Gulf of Guinea province of West Africa: US Geological Survey Bulletin 2207-C, 32.

BULL, S., CARTWRIGHT, C. & HUUSE, M. (2009). A review of kinematic indicators from mass- transport complexes using 3D seismic data. Marine & Petroleum Geology, 26, 1132 – 1151.

CARTWRIGHT, J.A., (1994). Episodic basin-wide hydrofracturing of overpressured early Cenozoic mudrock sequences in the North Sea Basin. *Marine and Petroleum Geology 11,* 587–607.

CARTWRIGHT, J.A. (2007). The impact of 3D seismic data on the understanding of compaction, fluid flow and diagenesis in sedimentary basins. *Journal of the Geological Society, London,* 164, 881.

CARTWRIGHT, J.A. (2011). Diagenetically induced shear failure of fine-grained sediments and the development of polygonal fault systems. *Marine and Petroleum Geology, 28,* 1593 – 1610.

CARTWRIGHT, J., HUUSE, M., APLIN, A., (2007). Seal bypass systems. *AAPG Bulletin 91,* 1141– 1166.

CAUQUIL, E., & ADAMY, J. (2008). Seabed imagery and chemosynthetic communities: Examples from deep offshore West Africa. Offshore Technology Conference, Houston.

CUNNINGHAM, R., & LINDHOLM, R.M.(2000). Seismic evidence for widespread gas hydrate formation, offshore west Africa. *AAPG Memoir 73,* 93–105.

DAVIES, R.J. (2003). Kilometer-scale fluidization structures formed during early burial of a deep-water slope channel on the Niger Delta. *Geology, 31,* 949 - 952.

DAVIES, R.J., & CLARK, I.R. (2006). Submarine slope failure primed and triggered by silica and its diagenesis. *Basin Research 18,* 339-350.

DAVIES, R. J., HUUSE, M., HURST, P., CATWRIGHT, J. & YANG, Y. (2006). Giant clastic intrusions primed by silica diagenesis. *Geology, 34*, 917-920.

DYKSTRA, M., FILDANI, A., MOSCARDELLI, L, CLARK, J., GERBER., T & OCHOA, J (2014). Predictive tools for deep-water depositional environments. SEPM workshop, Houston.

MARTÍNEZ, J.F., BERTONI, C., GÉRARD, J., & MATÍAS, H. (2011). Processes of submarine slope failure and fluid migration on the Ebro continental margin: implications for offshore exploration and development In: Shipp, R.C., Weimer, P., & Posamentier, H.W. (eds). Mass transport deposits in deep-water settings. *SEPM Special Publication 96, 181-198*

MARTINEZ, J.F., CARTWRIGHT, J., HALL, B. (2005). 3D seismic interpretation of slump complexes: examples from the continental margin of Israel. *Basin Research 17,*83–108.

GAY, A., LOPEZ, M., BERNT, C., & SERANNE, M. (2007). Geological controls on focused fluid flow associated with seafloor seeps in the Lower Congo Basin: Marine Geology 224, 68-92

GAY, A., LOPEZ, M., COCHONAT, P., SERMONDADAZ, G., (2004). Polygonal faults-furrows sys- tem related to early stages of compaction—upper Miocene to recent sediments of the Lower Congo *Basin. Basin Research 16, 101–11*

GAY, A., LOPEZ, M., COCHONAT, P., LEVACHÉ, D., SERMONDADAZ, G., SERANNE, M. (2006a). Evidences for early to late fluid migration from an upper Miocene turbiditic channel revealed by 3D seismic coupled to geochemical sampling within seafloor pockmarks, Lower Congo Basin. *Marine and Petroleum Geology 23,* 387–399.

GAY, A., LOPEZ, M., COCHONAT, P., SÉRANNE, M., LEVACHÉ, D., SERMONDADAZ, G., (2006b). Isolated seafloor pockmarks linked to BSRs, fluid chimneys, polygonal faults and stacked Oligocene–Miocene turbiditic palaeochannels in the Lower Congo Basin. Marine Geology 226, 25– 40.

GAY, A., LOPEZ, M., ONDREAS, H., CHARLOU, J.-L, SERMONDADAZ, G., & COCHONAT, P., (2006c). Seafloor facies related to upward methane flux within a Giant pockmark of the Lower Congo Basin. Marine Geology 226, 81-95.

GAY, A., LOPEZ, M., COCHONAT, P., SULTAN, N., CAUQUIL, E., & BRIGAUD, F (2003). Sinuous pockmark belt as indicator of a shallow buried turbiditic channel on the lower slope of the Congo basin, West African margin. In: Van Rensbergen, P., Hillis, R.R. & Morley, C.K. (eds) Subsurface Sediment Mobilization. *Geological Society, London, Special Publications, 216,* 173–189.

GEE, M.J.R & GAWTHORPE, R.L (2007). Early evolution of submarine channels offshore Angola revealed by three-dimensional seismic data. *Geological Society of London, Special Publication, 27,* 223-235

GOULTY, N.R (2001). Polygonal fault networks in fine-grained sediments an alternative to the syneresis mechanism. *First break 19,* 69-73

GRAUE, K., (2000). Mud volcanoes in deepwater Nigeria. *Marine and Petroleum Geology 17,* 959– 974

GREENHALGH, J., WELLS, S., BORSATO,. R., PRATT, D., MARTIN, M., ROBERSON., R., FONTES., & OBAJE, W.A. (2011). A fresh look at prospectivity of the Equatorial Conjugate Margin of Brazil and Africa. First Break, 29, 67-72.

HEGGLAND, R., (1998). Gas seepage as an indicator of deeper prospective reservoirs. A study based on exploration 3D seismic data. *Marine and Petroleum Geology 15,* 1–9.

HO, S., CATWRIGHT, J & IMBERT, P. (2012). Vertical evolution of fluid venting structures in relation to gas flux, in the Neogene-Quaternary of the Lower Congo Basin, Offshore Angola. *Marine Geology, 332-334,* 40-55.

HOVLAND, M. (2005). Gas hydrates. *Petroleum geology, 4,* 261 – 268.

HOVLAND, M., JUDD, A.G. 1988). Seabed Pockmarks and Seepages: Impact on Geology, Biology and the Marine Environment.

HUSTOFT, S., BÜNZ, S., MIENERT, J. (2010). Three-dimensional seismic analysis of the morphology and spatial distribution of chimneys beneath the Nyegga pockmark field, offshore mid- Norway. *Basin Research 22,* 465–480.

HUUSE, M., JACKSON, C.A.-L., RENSBERGEN, P. V., DAVIES, R.J., FLEMINGS, P.B. & DIXON, R.J. (2010). Subsurface sediment remobilization and fluid flow in sedimentary basins: an overview: *Basin Research, 22,* 342-360.

JUDD, A., HOVLAND, M. (2007). Seabed fluid flow - the impact on geology, biology and the marine environment. Cambridge University Press, 475.

KILHAMS, B., MCARTHUR, A., HUUSE, M., ITA, E., HARTLEY, A., (2011). Enigmatic large-scale furrows of Miocene to Pliocene age from the central North Sea: current-scoured pockmarks? *Geomarine Letters 31*, 437–449.

KING, L.H., MACLEAN, B. (1970). Pockmarks on the Scotian Shelf. *Geological Society of American Bulletin 81,* 3141–3148.

LIGTENBERG, J.H. (2005). Detection of fluid migration pathways in seismic data: implications for fault seal analysis. *Basin Research, 17*. 141-153.

LONERGAN, L., CARTWRIGHT, J. & JOLLY, R. (1998). The geometry of polygonal fault systems in Tertiary mudrocks of the North Sea. *Journal of the Geological Society, 83, 529-548.*

LONERGAN, L., & CARTWRIGHT, J. (1999). Polygonal faults and their influence on deep-water depositional sandstone reservoir geometries , Alba Field United Kingdom Central North Sea. *AAPG Bulletin 83, 410–432.*

LØSETH, H., WENSAAS, L., ARNTSEN, B., HANKEN, N., BASIRE, C., GRAUE, K., (2001). 1000 m long gas blow-out pipes. 3rd EAGE Conference & Exhibition, Amsterdam, Extended Abstracts, 524.

LØSETH, H., GADING, M., WENSAAS, L. (2009). Hydrocarbon leakage interpreted on seismic data. *Marine and Petroleum Geology 26,* 1304–1319.

LØSETH, H., WENSAAS, L., ARNTSEN, B., HANKEN, N., BASIRE, C., GRAUE, K. (2011). 1000 m long gas blow-out pipes. *Marine and Petroleum Geology 27,* 1047–1060.

MACGREGOR, D.S., ROBINSON, J., AND SPEAR, G. (2003). Play fairways of the Gulf of Guinea transform margin, *in* Arthur, T.J., MacGregor, D.S., and Cameron, N.R., eds., Petroleum geology of Africa—New themes and developing technologies: *Geological Society, London, Special Publication 207,* 289.

MECKEL, L. D (2011). Reservoir characteristics and classification of sand-prone submarine mass-transport deposits. In: Shipp, R.C., Weimer, P., & Posamentier, H.W. (eds). Mass transport deposits in deep-water settings. *SEPM Special Publication 96, 423-45266.*

MITCHUM JR., R.M., VAIL, P.R., SANGREE, J.B. (1977). Seismic stratigraphy and global changes of sea-level, part 6: stratigraphic interpretation of seismic reflection patterns in de- positional sequences. In: Payton, C.E. (Ed.), Seismic Stratigraphy—Applications to Hydrocarbon Exploration: *AAPG Memoir, 26,* 117–133.

MOSCARDELLI, L.,WOOD, L.&MANN, P. (2006). Mass-transport complexes and associated processes in the Offshore Area of Trinidad and Venezuela. *AAPG Bulletin, 90, 1059*-1088.

MOSCARDELLI, L. & WOOD, L. (2008). New classification system for mass transport complexes in offshore Trinidad. *Basin Research 20,* 73 – 98.

MOSS, J.L., CARTWRIGHT, J., (2010). The spatial and temporal distribution of pipe formation, offshore Namibia. *Marine and Petroleum Geology 27,* 1216–1234.

NELSON, C.H., ESCUTIA, C., DAMUTH., J.E., & TWICHELL (Jr), D.C. (2011). Interplay of mass-transport and turbidite-system deposits in different active tectonic and passive continental margin settings: external and local controlling factors. In: Shipp, R.C., Weimer, P., & Posamentier, H.W. (eds). Mass transport deposits in deep-water settings. *SEPM Special Publication 96, 39-66.*

NISSEN, S.E., HASKELL, N.L., STEINER, C.T., COTERILL, K.L., (1999). Debris flow outrunner blocks, glide tracks, and pressure ridges identified on the Nigerian continental slope using 3-D seismic coherency. The Leading Edge 18, 595–599.

OBAJE, N.G. (2009). The Dahomey Basin. Geology and Mineral Resources of Nigeria, Lecture Notes in Earth Sciences 120, 103-108.

OSTANIN, I., ANKA, Z., DI PRIMIO, R., BERMAL, A., (2012) Hydrocarbon leakage above the Snøhvit gas field, Hammerfest Basin SW Barents Sea. *First Break, 30*, 55-6.

PETROLEUM GEO-SERVICES (2006). Techlink, a PGS Geophysical, 6, 2.

PILCHER, R., ARGENT, J. (2007). Mega-pockmarks and linear pockmark trains on the West African continental margin. *Marine Geology 244,* 15–32.

POSAMENTIER, H. W & KOLLA, V. (2003). Seismic geomorphology and stratigraphy of depositional elements in deep-water settings. *Journal of Sedimentary Research, 73, 3,* 367 – 388.

POSAMENTIER, H. W & MARTINSEN, O.J (2011). The character and genesis of submarine mass-transport deposits: insights from outcrop and 3d seismic data. In: Shipp, R.C., Weimer, P., & Posamentier, H.W. (eds). Mass transport deposits in deep-water settings. *SEPM Special Publication 96, 7-38.*

REICHE, S., HJELSTUEN, B.O & HAFLIDASON. H (2011). High-resolution seismic stratigraphy, sedimentary processes and the origin of seabed cracks and pockmarks at Nyegga, mid-Norwegian margin. *Marine Geology, 284,* 28-39.

RISE, L., SÆTTEM, J., FANAVOLL, S., THORSNES, T., OTTESEN, D., BØE, R., (1999). Sea-bed pockmarks related to fluid migration from Mesozoic bedrock strata in the Skagerrak offshore Norway. *Marine and Petroleum Geology 16,* 619–631.

SCHROOT, B.M. & SCHÜTTENHELM, R.T.E. (2003). Expressions of shallow gas in the Netherlands North Sea. *Netherlands Journal of Geosciences, 82,* 91-105.

SERIÉ, C., HUUSE, M., SCHØDT, N. (2012). Gas hydrate pingoes: deep seafloor evidence of focused fluid flow on continental margins. *Geology 40*, 207–210.

SHIPLEY, T.H., HOUSTON, M.,H., BUFFLER, R.T., SHAUB, F.J., McMILLEN, K.J., LADD,J.W., and WORZEL, J.L. (1979). Seismic evidence of widespread possible gas hydrate horizons on continental slopes and rises: *AAPG Bulletin, 63,* 2204-2213.

SHIPP, R.C., WEIMER, P., & POSAMENTIER, H.W. (2011). Mass transport deposits in deep-water settings: an introduction. In: Shipp, R.C., Weimer, P., & Posamentier, H.W. (eds). Mass transport deposits in deep-water settings. *SEPM Special Publication 96, 3-6.*

SHOULDERS, S.J., CARTWRIGHT, J. & HUUSE, M. (2007). Large scale conical sandstone intrusions and polygonal fault systems in Tranche 6, Faroe-Shetland basin. *Marine & Petroleum Geology, 24,* 173-188.

STEWART, S.A. (1999). Seismic interpretations of circular geological structures. *Petroleum Geoscience, 5,* 273-285.

STUEVOLD, L.M., FAERSETH, R.B., ARNESEN, L., CARTWRIGHT, J. & MO¨LLER, N. (2003). Polygonal faults in the Ormen Lange Field, Møre Basin, offshore Mid-Norway. In: Van Rensbergen, P., Hillis, R.R. & Morley, C.K. (eds) Subsurface Sediment Mobilization. *Geological Society, London, Special Publications, 216,* 263–281.

SULTAN, N., MARSSET, B., KER, S., MARSSET, T., VOISSET, M., VERNANT, A.M., BAYON, G., CAUQUIL, E., ADAMY, J., COLLIAT, J.L., DRAPEAU, D., (2010). Hydrate dissolution as a potential mechanism for pockmark formation in the Niger delta*. Journal of Geophysical Research*, *113,* 1 – 33.

SUTTON, J.P., & MITCHUM, R.M. Jr (2011). Upper Quaternary seafloor mass-transport deposits at the base of slope, offshore Niger Delta, deep-water Nigeria. In: Shipp, R.C., Weimer, P., & Posamentier, H.W. (eds). Mass transport deposits in deep-water settings. *SEPM Special Publication 96, 85-110.*

VANNESTE, M., MIENERT, J., BUNZ, S. (2006). The Hinlopen Slide: A giant, submarine slope failure on the northern Svalbard margin, Arctic Ocean. *Earth and Planetary Science Letters 245*, 373–388.

VAN RENSBERGEN, P., HILLIS, R.R., MALTMAN, A.J., MORLEY, C.K. (Eds.), (2003a) Subsurface Sediment Mobilization: *Geological Society Special Publications, Geological Society, London, Special Publications, 216.*

ZHU, M., GRAHAM.S., & McHARGUE, T. (2011). Characterization of mass-transport deposits on a Pliocene siliciclastic continental slope, North western South China Sea. In: Shipp, R.C., Weimer, P., & Posamentier, H.W. (eds). Mass transport deposits in deep-water settings. *SEPM Special Publication 96, 111-125.*

ZIEGLER, P.A. ed. (1988) Evolution of the Arctic-North Atlantic and the Western Tethys. The American Association of Petroleum Geologists, Tulsa, OK, USA. *AAPG Memoir 43.*

FIGURE AND TABLE CAPTIONS

Fig. 1(a) *Gulf of Guinea Province (7183) with location of oil and gas fields shown in red outline;* ***(b)*** *Structural zones along the West African transform Margin and location of study area. The area covers OPL blocks 312, 313 and 314 as show in red. Yellow and blue boxes represent location of soft-sediment deformation features and fluid flow pipes by Davies 2003 & Løseth et al., 2011 respectively, Aje field and Ogo discoveries also shown. Area falls within the frontal deformation zone. Inset shows location with the Atlantic (Redrawn from Brownfield & Charpentier 2006; Techlink, PGS 2006).*

Fig. 2*. Simplified stratigraphic column and petroleum systems along the West African Transform Margin (adapted from Borsato et al., 2012). Also shown is the occurrence of MTDs and fluid flow features observed from the study area from this study.*

Fig. 3 *TWT structure map of the seabed topography showing the extent of the 3D seismic data used for study. Entire study area is divided into 2 areas for ease of description and discussion. Division is based on approximate extent of MTDs and fluid flow deposits (depth range c. 1350-2700 m).*

Fig. 4a*. Dip line across the study area showing major surfaces and units. Surfaces extended from Aje field towards the northern part of the survey (PGS). Location of line shown on seabed map*

Fig. 4b-e. *Strike and random dip lines across the study area showing seismic units and surfaces. Units are defined based on seismic facies and terminations. Units are extensively deformed into mass transport deposits.*

Fig. 5. *TWT thickness maps of the mapped seismic units.*

Fig. 6 *Dip angle and variance attribute maps to show the topography of seabed. Depositional, soft-sediment deformation and fluid flow features such as, submarine channels, sediment waves, mass transport deposits, pockmarks and mound are well imaged.*

Fig. 7 *Summary diagrams of key components of the mass transport deposits along the Nigeria Transform Margin often used for kinematic indication*

Fig 8. *Mass transport deposits in the area* ***(a)*** *seafloor topography showing components of series of mass transport deposits. At least 3 are identified. Image also reveals other seafloor features such as*

meandering and straight channels, pockmarks, faults and mound. Red arrow shows transport direction of failed sediments down south ***(b)*** *seismic section through the headwall scarp of MTD 2. Note how fault cuts through the sediments* ***(c)*** *dip seismic line revealing all three MTDs on the seafloor. Headwall scarps and lateral margins are well imaged. High-amplitude reflections observed directly beneath the seabed and above the faulted structural high. Line locations for b and c shown in a.*

Fig. 9. (a&b) *Seismic profile showing well- preserved, deformed MTD blocks and other features* ***(c)*** *variance extracted on top surface of deformed blocks*

(d) *time structure map of base of SU5 showing MTD ramps.*

Fig. 10 *Evolution and distribution of MTDs along the Nigerian Transform Margin during the Cenozoic. Coloured patches represent single MTD drawn from its basal surface in petrel. Deformation increases with time. Note that outline of seabed MTDs are not included*

Fig 11*. Iso-proportional slicing through a frequency decomposition colour blend volume* ***(a)*** *W-E seismic section showing location of slices (time 10 – time 1) from the seabed to the base of the channel complexes, Cc* ***(b)*** *individual iso-slice to image channels. At least five channel complexes/belts are observed. Cc1 is meandering and confined within the belt but Cc2 - 4 are disorganised. Cc5 forms a linear channel complex belt. Note location of seabed mound above paleo channels. MTDs are also observed.*

Fig. 12. (a & b) *TWT surface and RMS attribute map of the seabed to image linear channels. Channels react near structural high; they merge and bifurcate downslope forming two more channels* ***(c-f)*** *seismic profiles downslope across channels* ***(g)*** *dip map of the seabed showing the linear channels*

Fig. 13. *Sediment waves* ***(a)*** *RMS amplitude map @ 50 ms TWT below the present day seabed showing morphology of sediment wave. Transport direction is NE – SW as the channels* ***(b)*** *cross section through the train of sediment wave* ***(c & d)*** *dip and random lines showing how the reflections interpreted as sediment waves are constrained within the channel margin. Note presence of polygonal faults. Location of lines shown in "a"*

Fig. 14*. Isolated pipes and pockmarks above a structural high in the northern part of the study area* ***(a)*** *seismic section through vertical columns and depressions on the seafloor interpreted as pipes and pockmarks respectively. Inset shows the circular to oval planform geometry @ -1808 ms twt* ***(b)*** *Dip angle map of the seafloor reveals the distribution of pockmarks* ***(c-g)*** *isolated pockmarks and underlying pipe anomalies. Locations shown in b. Note the occurrence of high- amplitude anomalies below pipes, along fault planes and above structural. Anomalies are possible gas accumulations*

Fig.15*. Seismic expression of pockmarks* ***(a)*** *stacked pockmarks and schematic diagram* ***(b)*** *surface of individual level of stacked pockmarks. Note how it deepens and widens with depth* ***(c)*** *another example of stacked pockmarks* ***(d - f)*** *pockmarks associated with fault,* ***(d)*** *above the fault plane* ***(e)***

*along hanging wall of fault **(f)** TWT and attribute maps on the seabed showing planview expression of pockmarks and faults*

***Fig. 16** Presence of pockmarks above active and paleochannels. **(a)** variance attribute extracted on the present day seabed. Pockmarks (red arrows) are randomly distributed within the present day channel-belt complex and above paleochannels. Location of seismic sections shown **(b)** line through the main channel-belt complex. Pockmarks occur above channel margins **(c)** seismic line across the main channel-belt. Pockmarks occur within and away from it **(d & e)** pockmarks on the seabed above paleochannels. Fluids could have migrated through porous sands within the channels or along faults to the seabed to create pockmarks*

***Fig. 17**. **(a)** 3D image with seismic cross section and RMS attribute extracted on the yellow horizon with a window length of 25 ms to reveal circular and elongate plan view geometries of high-amplitude, wedge-shaped anomalies **(b)** profile through isolated pockmarks **(c)** plan view geometry showing relationship between circular and elongated pockmarks and location of seismic profiles **(d)** Seismic profile in 16a showing relationship between the deep-seated, regional faults and high-amplitude, wedge-shaped anomalies. Shallow interval also affected by polygonal faults. Inset shows transition from circular pockmark to elongated pockmarks due to fault interaction. Note presence of BSR*

***Fig. 18a&b**. Seismic and interpreted section showing BSR **(c&d)** pockmarks occur above BSR and interval is polygonally faulted. Note presence of free gas below **(e)** 3D image showing relationship between BSR and faults in the area. BSR (black lines) were mapped only on lines where they clearly crosscut the stratigraphy*

***Fig.19**. Seabed mound **(a)** variance extraction on the seabed showing mound and other seafloor features **(b)** dip seismic line across the mound. Vertical column with distorted internal facies below the mound. Surrounding strata is unaffected by distortion **(c)** strike seismic line across the mound. High-amplitude intervals below the vertical column are paleo or buried channels **(d)** 3D image illustrating the relationship between the mound, underlying vertical column and sand-filled channels **(e)** time slices @ -2380, -2392 and -2404 ms TWT through the vertical column.*

***Fig 20. (a)** Seismic profile showing presence of polygonal faults networks with SU3-5 **(b)** seismic amplitude map of the green horizon showing polygonal geometry of the faults from paleoscan **(c&d)** close up of seismic line in (a) and variance (trace to trace discontinuity) attribute on the green horizon. Note how the faults are better imaged using variance. Polygonal fault orientation changes close to the major regional faults **(e)** time structure map and **(f)** variance attribute from the shallower section showing polygonal faults.*

***Fig. 21** Summary of depositional, soft-sediment remobilization/deformation and fluid flow elements observed along the Nigerian Transform Margin.*

Fig. 22 (a) *variance on seabed* ***(b-j)*** *schematic representations of seabed and overburden fluid flow features observed in area 1*

Fig. 23 *Graphical representation of estimated net sediment accumulation rate in area. Inset diagram represents spatial distribution of mass transport deposits in the area*

Table 1 *Key seismic data parameters such as frequency, velocity, horizontal and vertical resolution for each of the seismic units.*

Table 2. *Similarities and differences between polygonal faults in this study and other basins*

Table 3 *Estimated net sediment accumulation rates of Cretaceous till present day in NTM*

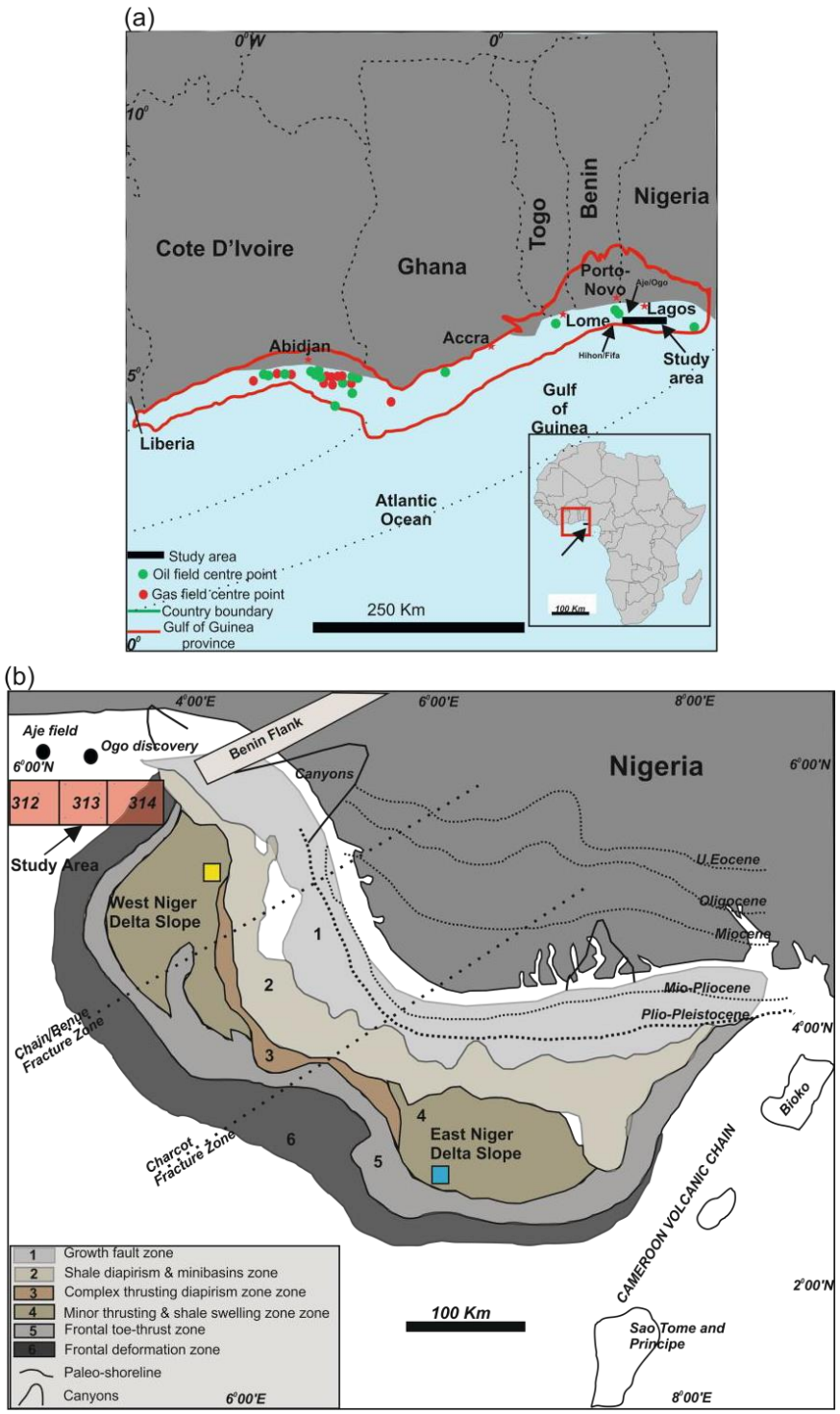
(a)
0°W
0°
10°
5°
0°
Cote D'Ivoire
Ghana
Togo
Benin
Nigeria
Porto-Novo
Aje/Ogo
Lagos
Lome
Accra
Abidjan
Hihon/Fifa
Study area
Gulf of Guinea
Liberia
Atlantic Ocean
Study area
Oil field centre point
Gas field centre point
Country boundary
Gulf of Guinea province
250 Km
100 Km
(b)
4°00'E
6°00'E
8°00'E
Aje field
Ogo discovery
6°00'N
Benin Flank
Canyons
Nigeria
312
313
314
Study Area
West Niger Delta Slope
U.Eocene
Oligocene
Miocene
Mio-Pliocene
Plio-Pleistocene
4°00'N
Chain/Benue Fracture Zone
Charcot Fracture Zone
East Niger Delta Slope
Bioko
CAMEROON VOLCANIC CHAIN
2°00'N
Sao Tome and Principe
1 Growth fault zone
2 Shale diapirism & minibasins zone
3 Complex thrusting diapirism zone zone
4 Minor thrusting & shale swelling zone zone
5 Frontal toe-thrust zone
6 Frontal deformation zone
Paleo-shoreline
Canyons
100 Km

Fig 1.

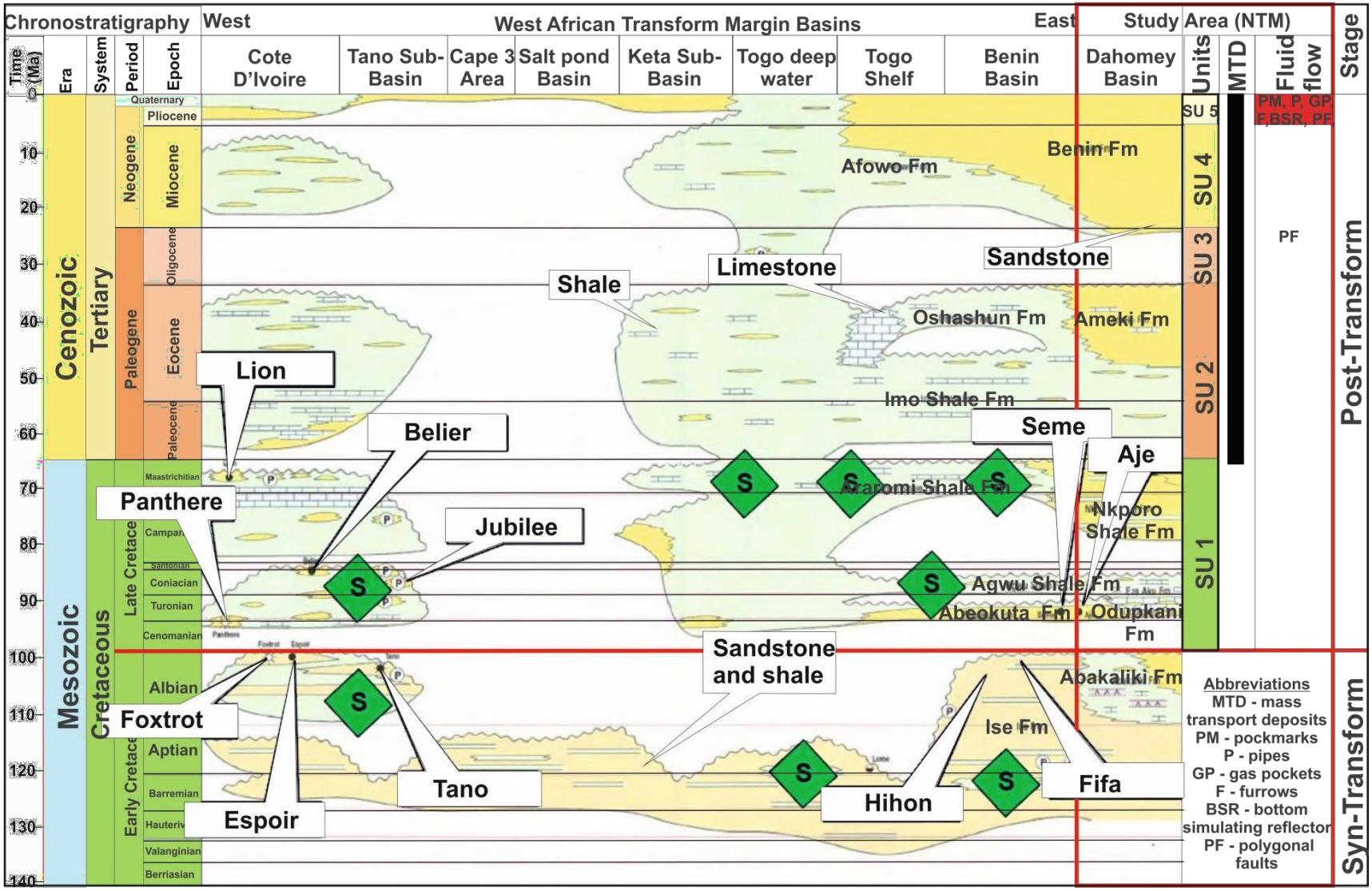
Chronostratigraphy
West
West African Transform Margin Basins
East
Study Area (NTM)
Time (Ma)
Era
System
Period
Epoch
Cote D'Ivoire
Tano Sub-Basin
Cape 3 Area
Salt pond Basin
Keta Sub-Basin
Togo deep water
Togo Shelf
Benin Basin
Dahomey Basin
Units
MTD
Fluid flow
Stage
Cenozoic
Tertiary
Neogene
Miocene
Pliocene
Quaternary
Paleogene
Oligocene
Eocene
Paleocene
Mesozoic
Cretaceous
Late Cretace
Early Cretace
Maastrichtian
Campan
Santonian
Coniacian
Turonian
Cenomanian
Albian
Aptian
Barremian
Hauteriv
Valanginian
Berriasian
Afowo Fm
Benin Fm
Sandstone
Limestone
Shale
Oshashun Fm
Ameki Fm
Imo Shale Fm
Seme
Aje
Araromi Shale Fm
Nkporo Shale Fm
Agwu Shale Fm
Abeokuta Fm
Odupkani Fm
Abakaliki Fm
Ise Fm
Lion
Belier
Panthere
Jubilee
Foxtrot
Espoir
Tano
Sandstone and shale
Hihon
Fifa
S
SU 5
SU 4
SU 3
SU 2
SU 1
PM, P, GP, F,BSR, PF
PF
Post-Transform
Syn-Transform
Abbreviations
MTD - mass transport deposits
PM - pockmarks
P - pipes
GP - gas pockets
F - furrows
BSR - bottom simulating reflector
PF - polygonal faults

Fig. 2

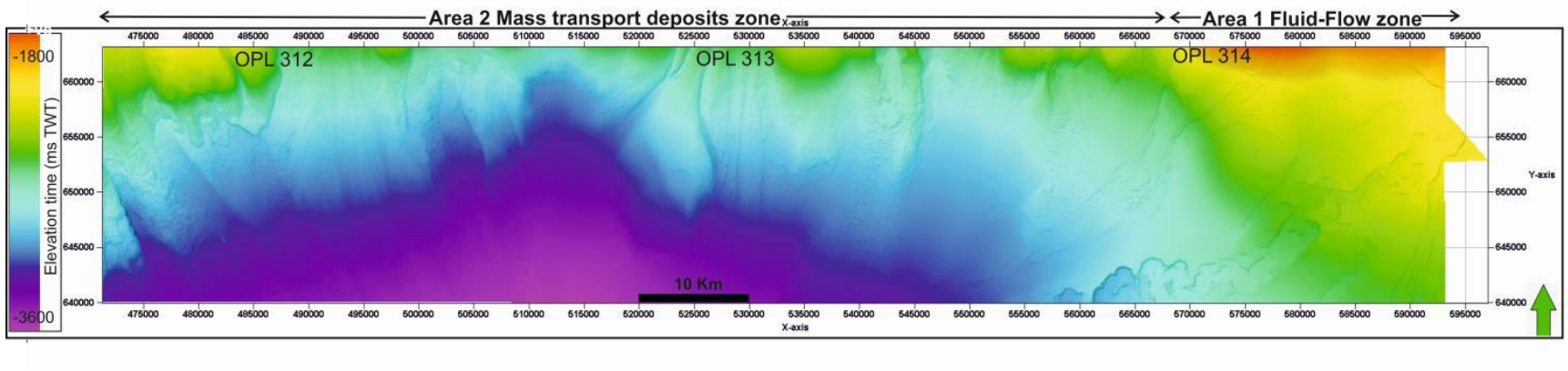
Area 2 Mass transport deposits zone
Area 1 Fluid-Flow zone
OPL 312
OPL 313
OPL 314
-1800
-3600
Elevation time (ms TWT)
10 Km
X-axis
Y-axis

Fig. 3

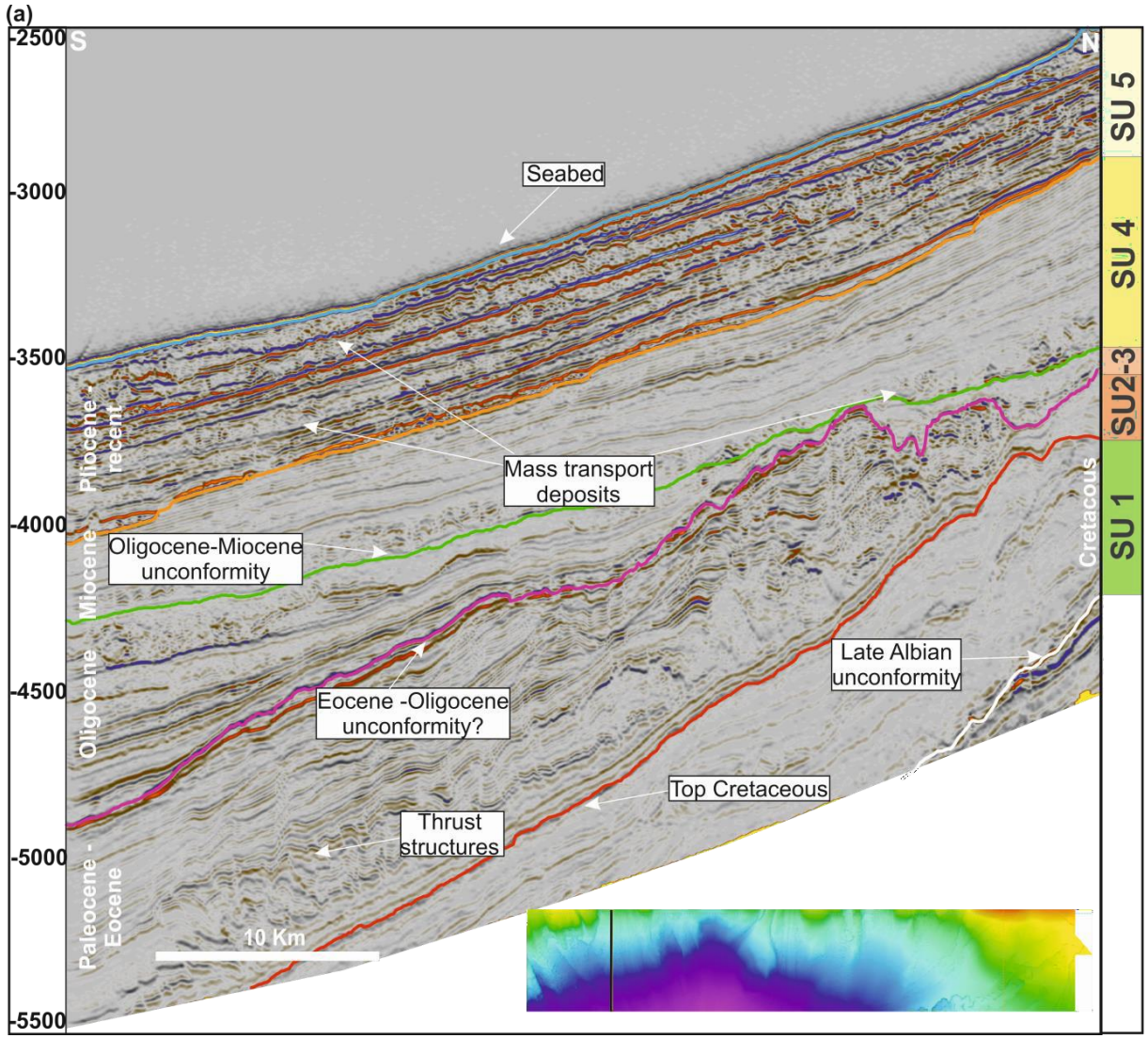
(a)
-2500
-3000
-3500
-4000
-4500
-5000
-5500
S
N
Seabed
Mass transport deposits
Oligocene-Miocene unconformity
Eocene -Oligocene unconformity?
Late Albian unconformity
Top Cretaceous
Thrust structures
Pliocene - recent
Miocene
Oligocene
Paleocene - Eocene
Cretaceous
10 Km
SU 5
SU 4
SU2-3
SU 1

Fig. 4a.

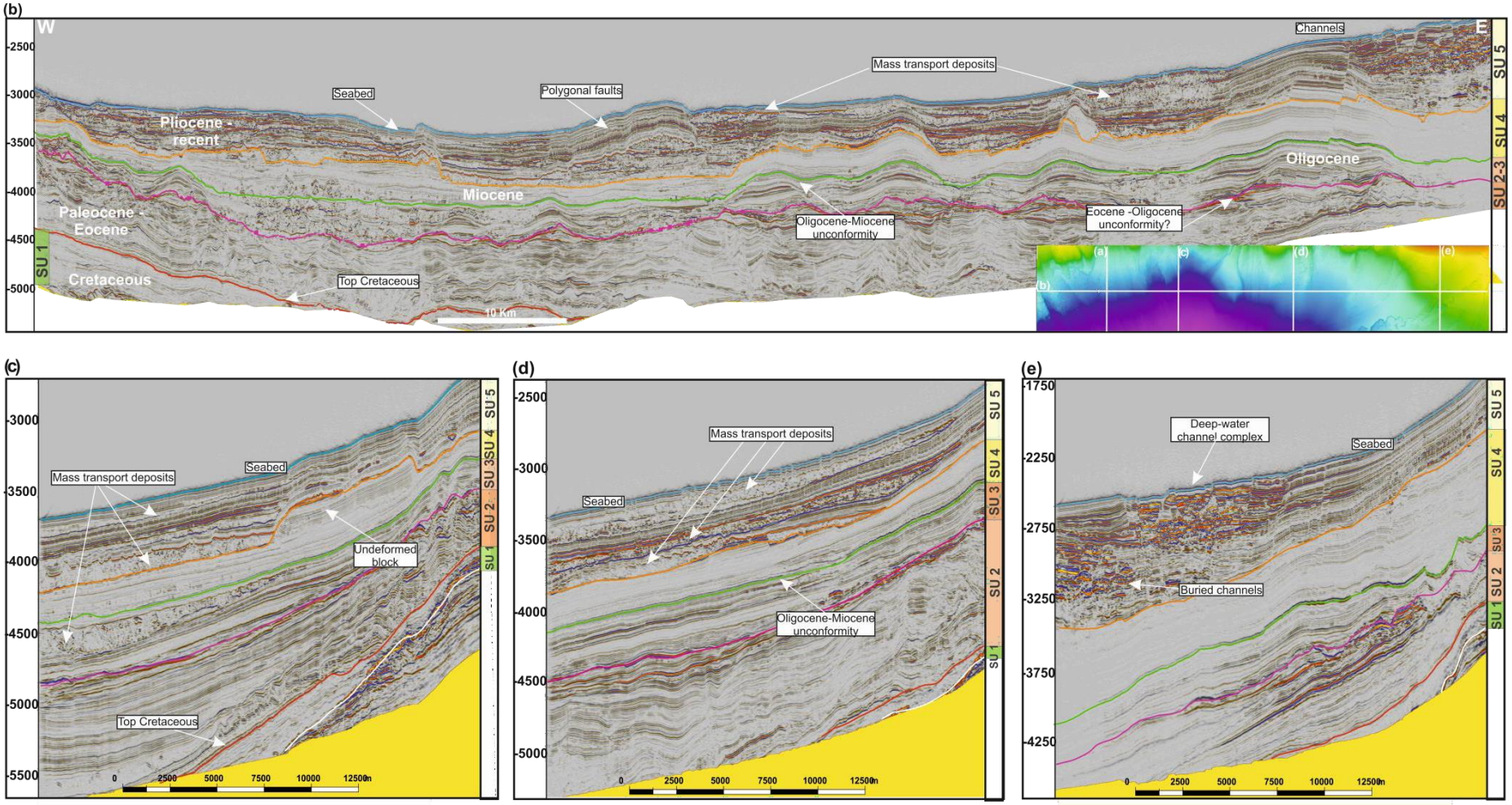
(b)
W
E
Channels
Mass transport deposits
Seabed
Polygonal faults
Pliocene - recent
Miocene
Oligocene
Paleocene - Eocene
Oligocene-Miocene unconformity
Eocene -Oligocene unconformity?
Cretaceous
Top Cretaceous
10 Km
SU 1
SU 2-3
SU 4
SU 5
(c)
Mass transport deposits
Seabed
Undeformed block
Top Cretaceous
(d)
Mass transport deposits
Seabed
Oligocene-Miocene unconformity
(e)
Deep-water channel complex
Seabed
Buried channels
0 2500 5000 7500 10000 12500m

Fig. 4b-e.

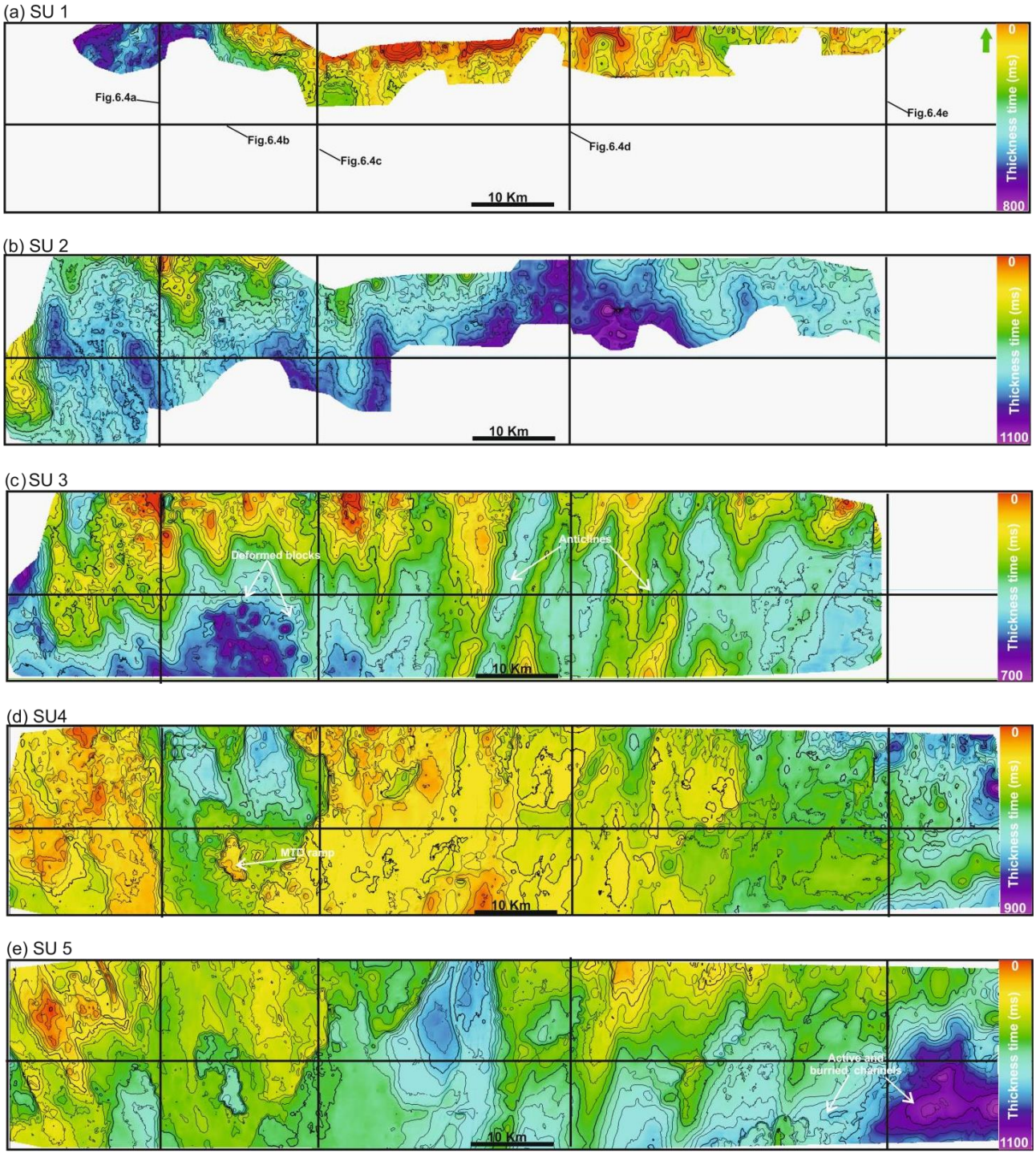
(a) SU 1
Fig.6.4a
Fig.6.4b
Fig.6.4c
Fig.6.4d
Fig.6.4e
10 Km
Thickness time (ms)
0
800
(b) SU 2
10 Km
Thickness time (ms)
0
1100
(c) SU 3
Deformed blocks
Anticlines
10 Km
Thickness time (ms)
0
700
(d) SU4
MTD ramp
10 Km
Thickness time (ms)
0
900
(e) SU 5
Active and buried channels
10 Km
Thickness time (ms)
0
1100

Fig. 5.

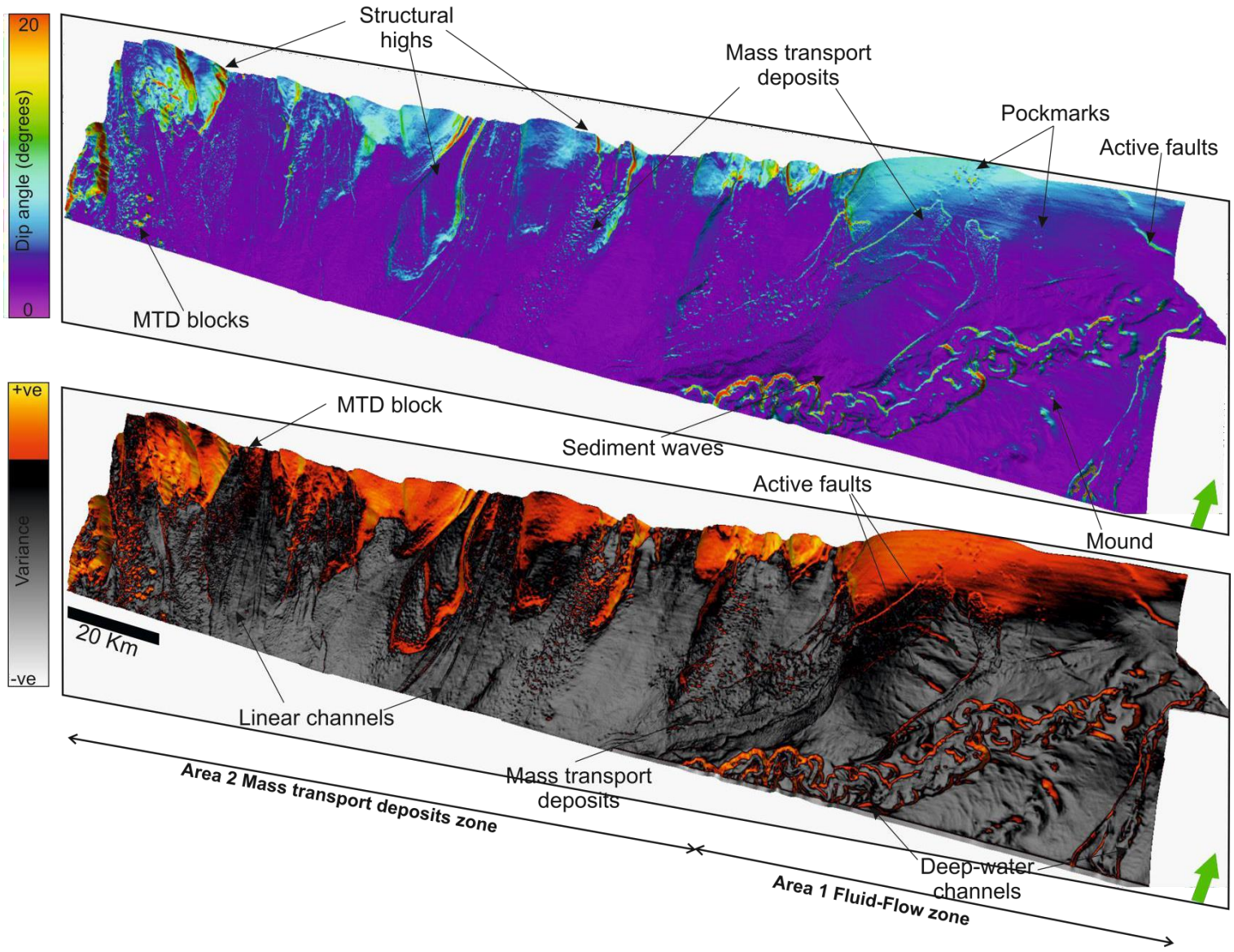
20
Dip angle (degrees)
0
Structural highs
Mass transport deposits
Pockmarks
Active faults
MTD blocks
+ve
Variance
-ve
MTD block
Sediment waves
Active faults
Mound
20 Km
Linear channels
Mass transport deposits
Deep-water channels
Area 2 Mass transport deposits zone
Area 1 Fluid-Flow zone

Fig. 6

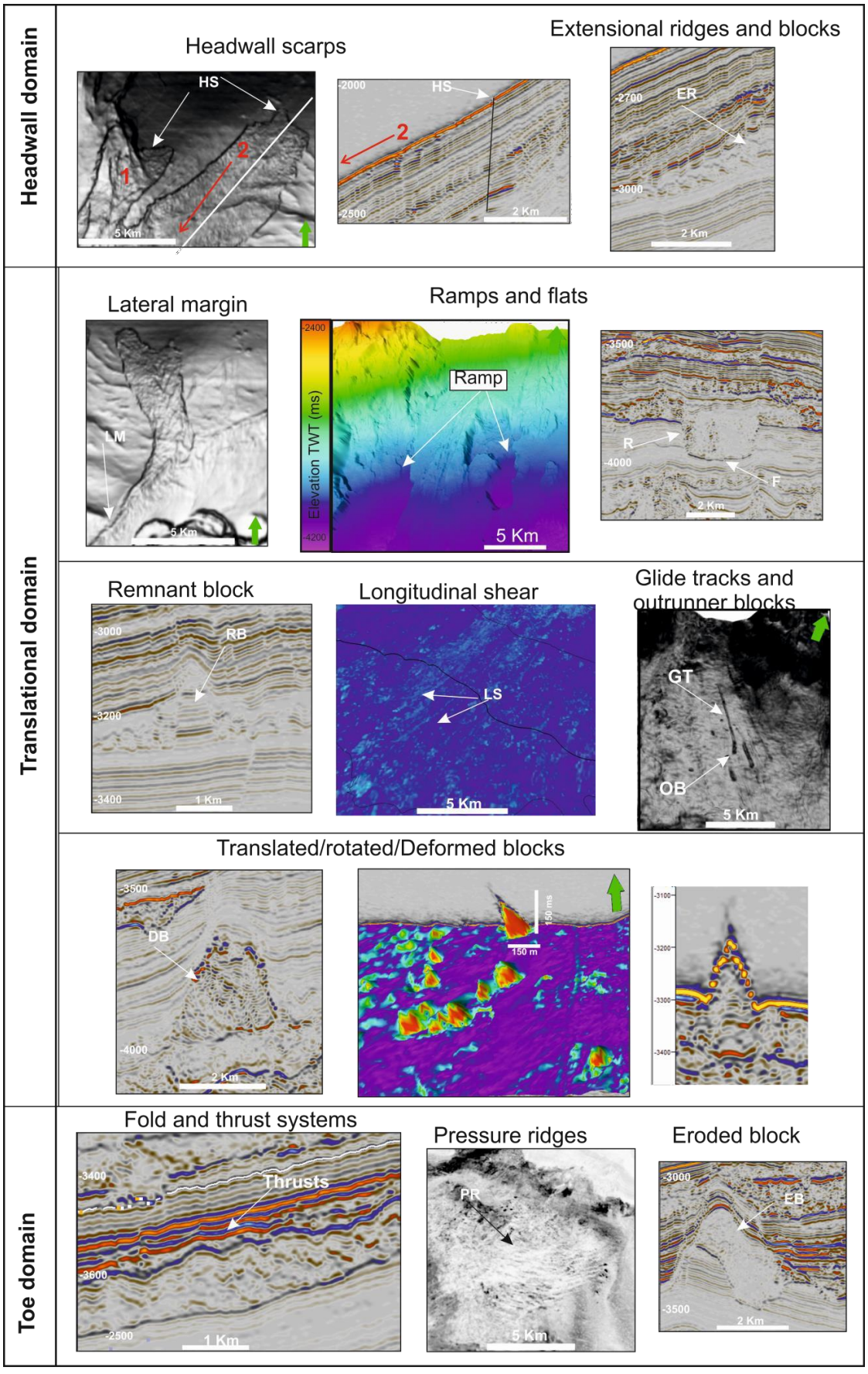
Headwall domain
Translational domain
Toe domain
Headwall scarps
HS
1
2
5 Km
-2000
-2500
2 Km
Extensional ridges and blocks
-2700
ER
-3000
2 Km
Lateral margin
LM
5 Km
Ramps and flats
2400
Elevation TWT (ms)
4200
Ramp
5 Km
-3500
R
-4000
F
2 Km
Remnant block
-3000
RB
-3200
-3400
1 Km
Longitudinal shear
LS
5 Km
Glide tracks and outrunner blocks
GT
OB
5 Km
Translated/rotated/Deformed blocks
-3500
DB
-4000
2 Km
150 ms
150 m
-3100
-3200
-3300
-3400
Fold and thrust systems
-3400
Thrusts
-3600
-2500
1 Km
Pressure ridges
PR
5 Km
Eroded block
-3000
EB
-3500
2 Km

Fig. 7

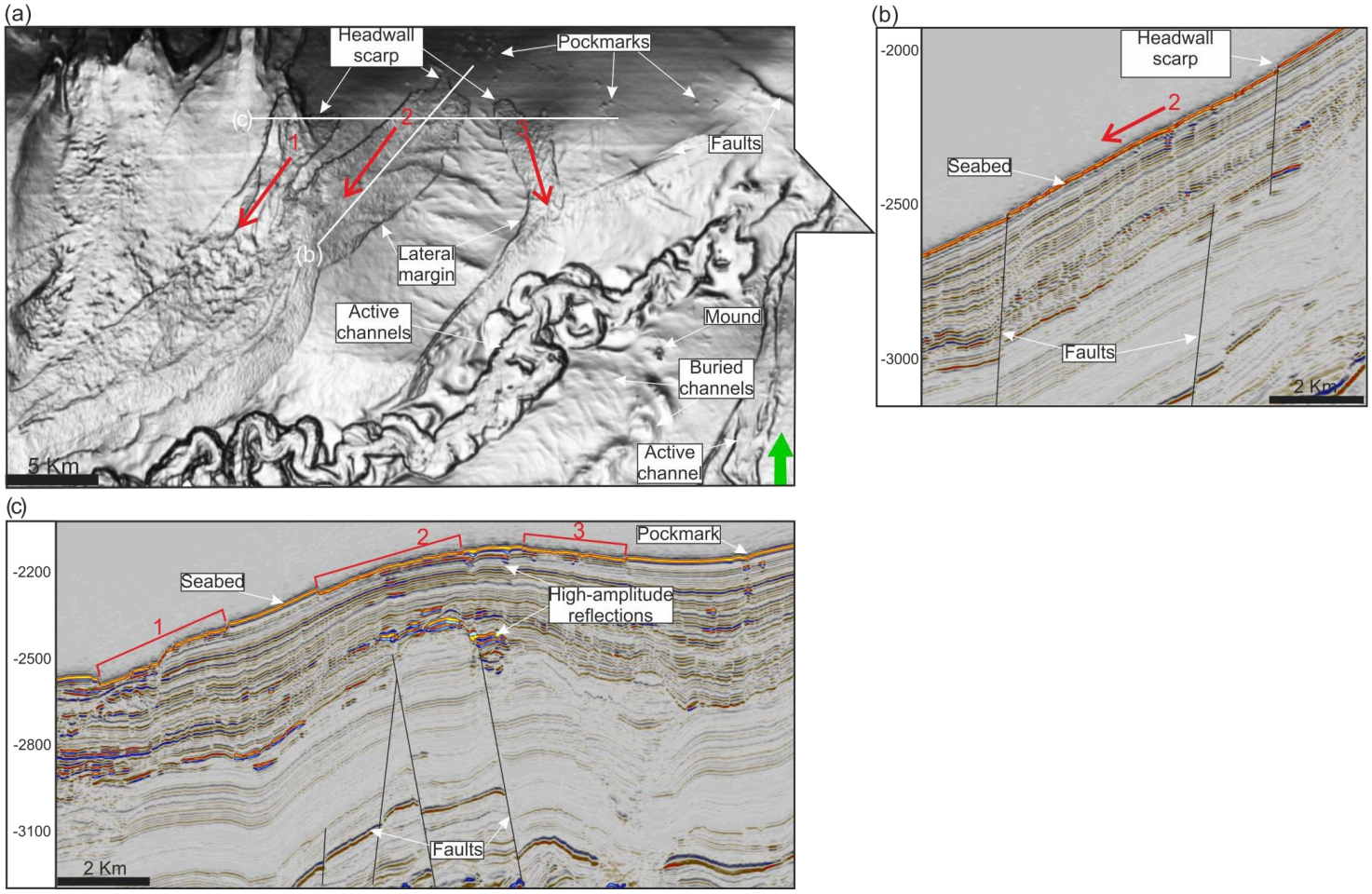
(a)
Headwall scarp
Pockmarks
(c)
1
2
3
Faults
(b)
Lateral margin
Active channels
Mound
Buried channels
Active channel
5 Km
(b)
-2000
-2500
-3000
Headwall scarp
2
Seabed
Faults
2 Km
(c)
-2200
-2500
-2800
-3100
Seabed
1
2
3
Pockmark
High-amplitude reflections
Faults
2 Km

Fig 8.

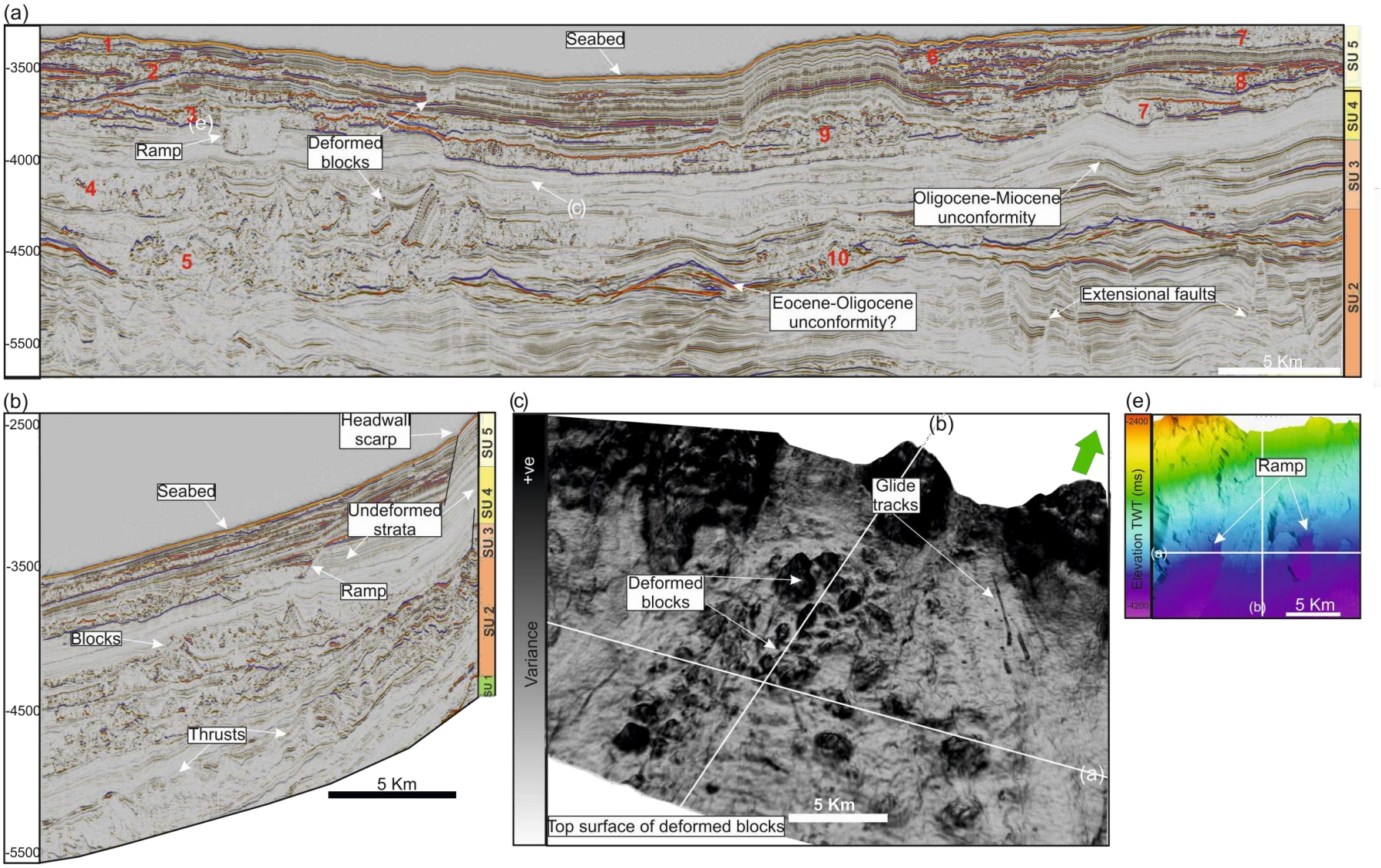
(a)
Seabed
Ramp
Deformed blocks
(e)
(c)
Oligocene-Miocene unconformity
Eocene-Oligocene unconformity?
Extensional faults
-3500
-4000
-4500
-5500
SU 5
SU 4
SU 3
SU 2
5 Km
(b)
Headwall scarp
Seabed
Undeformed strata
Ramp
Blocks
Thrusts
-2500
-3500
-4500
-5500
SU 5
SU 4
SU 3
SU 2
SU 1
5 Km
(c)
+ve
Variance
(b)
Glide tracks
Deformed blocks
(a)
5 Km
Top surface of deformed blocks
(e)
Ramp
Elevation TWT (ms)
-2400
-4200
(a)
(b)
5 Km

Fig. 9.

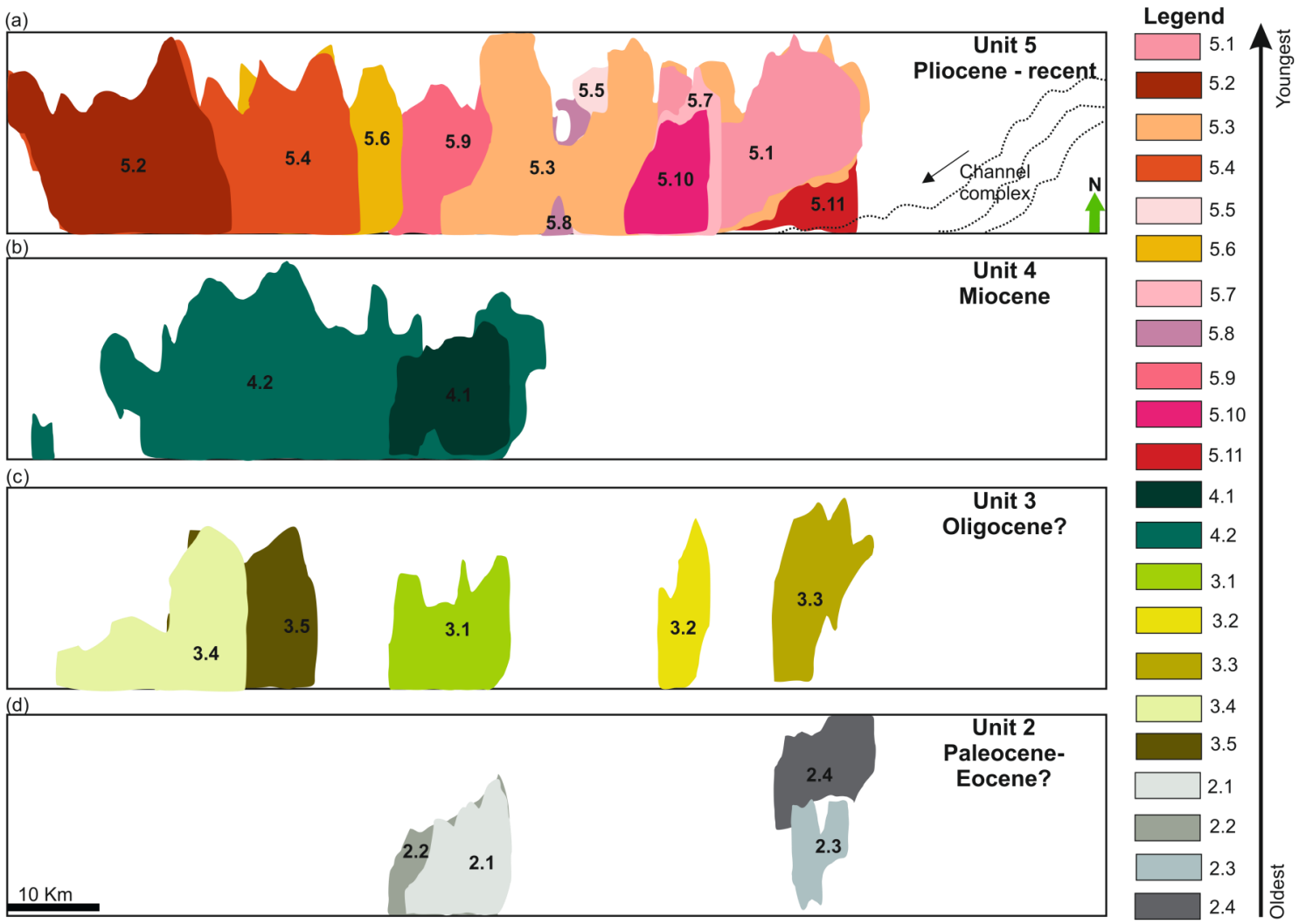
(a)
Unit 5
Pliocene - recent
5.2
5.4
5.6
5.9
5.3
5.5
5.8
5.7
5.10
5.1
5.11
Channel
complex
N
(b)
Unit 4
Miocene
4.2
4.1
(c)
Unit 3
Oligocene?
3.4
3.5
3.1
3.2
3.3
(d)
Unit 2
Paleocene-
Eocene?
2.2
2.1
2.4
2.3
10 Km
Legend
5.1
5.2
5.3
5.4
5.5
5.6
5.7
5.8
5.9
5.10
5.11
4.1
4.2
3.1
3.2
3.3
3.4
3.5
2.1
2.2
2.3
2.4
Youngest
Oldest

Fig. 10

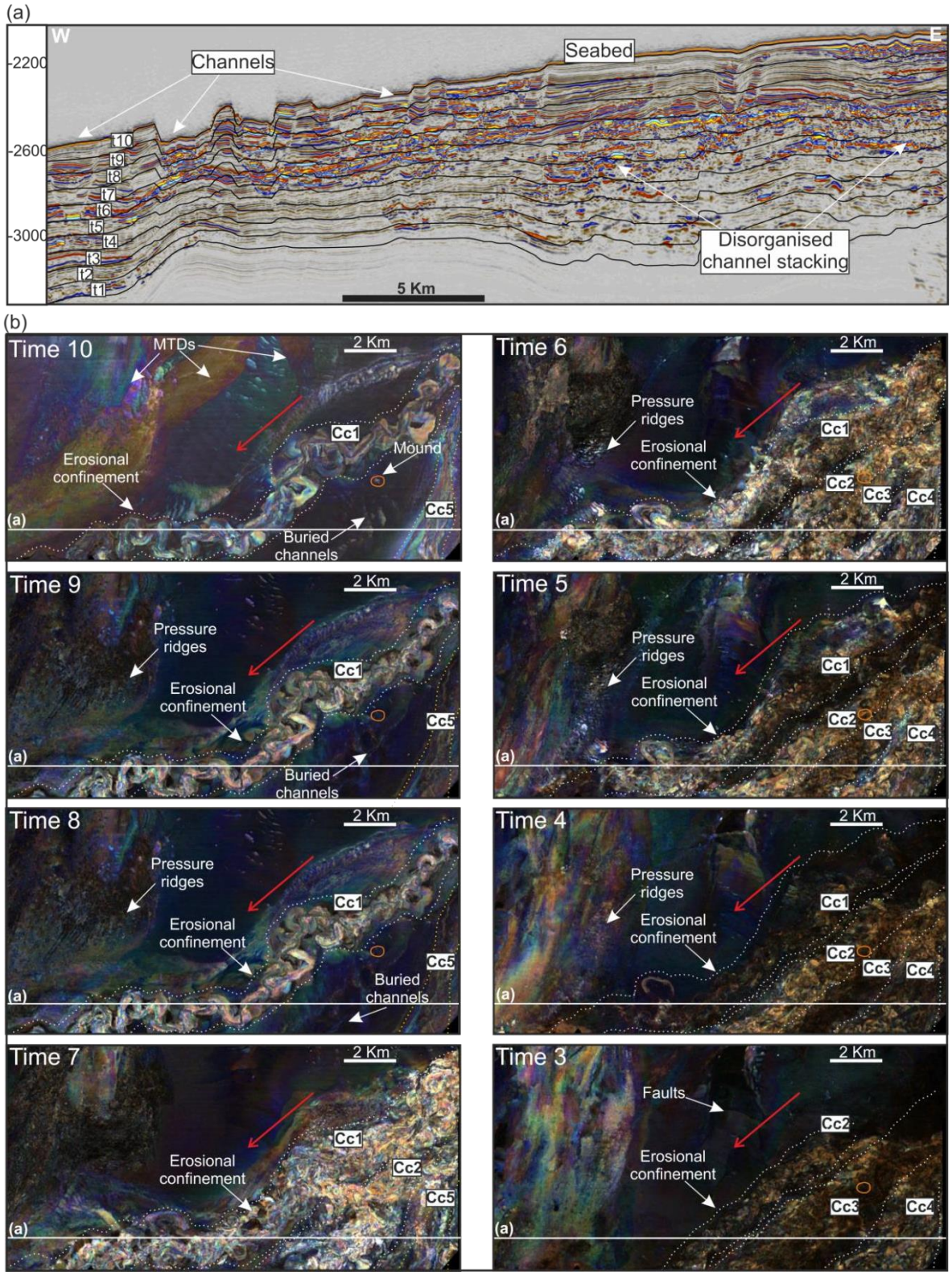
(a)
W
E
-2200
-2600
-3000
Channels
Seabed
t10
t9
t8
t7
t6
t5
t4
t3
t2
t1
Disorganised
channel stacking
5 Km
(b)
Time 10
MTDs
2 Km
Cc1
Mound
Erosional
confinement
Cc5
(a)
Buried
channels
Time 6
Pressure
ridges
Erosional
confinement
Cc2
Cc3
Cc4
Time 9
Time 5
Time 8
Time 4
Time 7
Time 3
Faults

Fig 11.

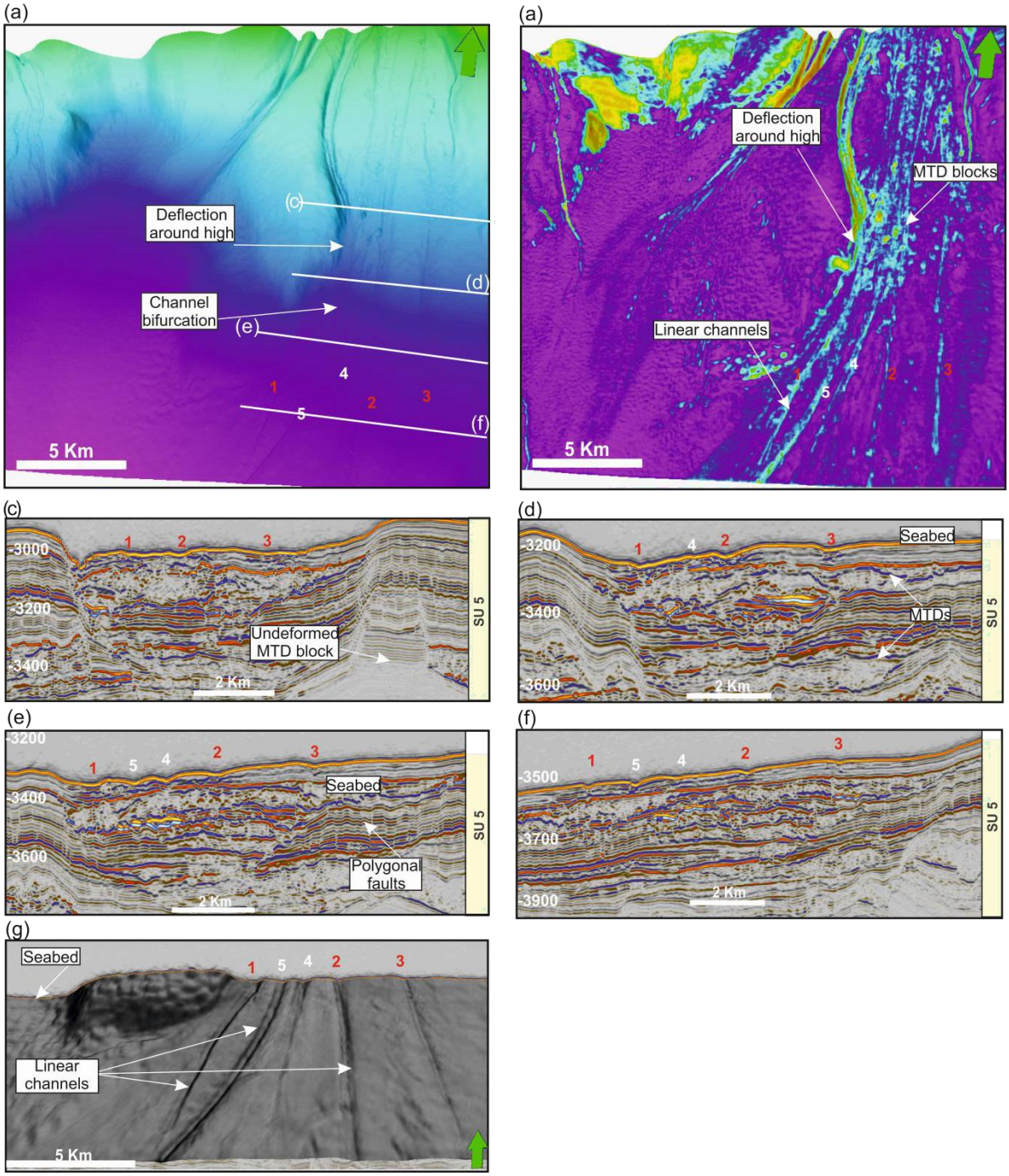
(a)
Deflection around high
(c)
(d)
Channel bifurcation
(e)
(f)
5 Km
(a)
Deflection around high
MTD blocks
Linear channels
5 Km
(c)
Undeformed MTD block
SU 5
2 Km
(d)
Seabed
MTDs
SU 5
2 Km
(e)
Seabed
Polygonal faults
SU 5
2 Km
(f)
SU 5
2 Km
(g)
Seabed
Linear channels
5 Km

Fig. 12

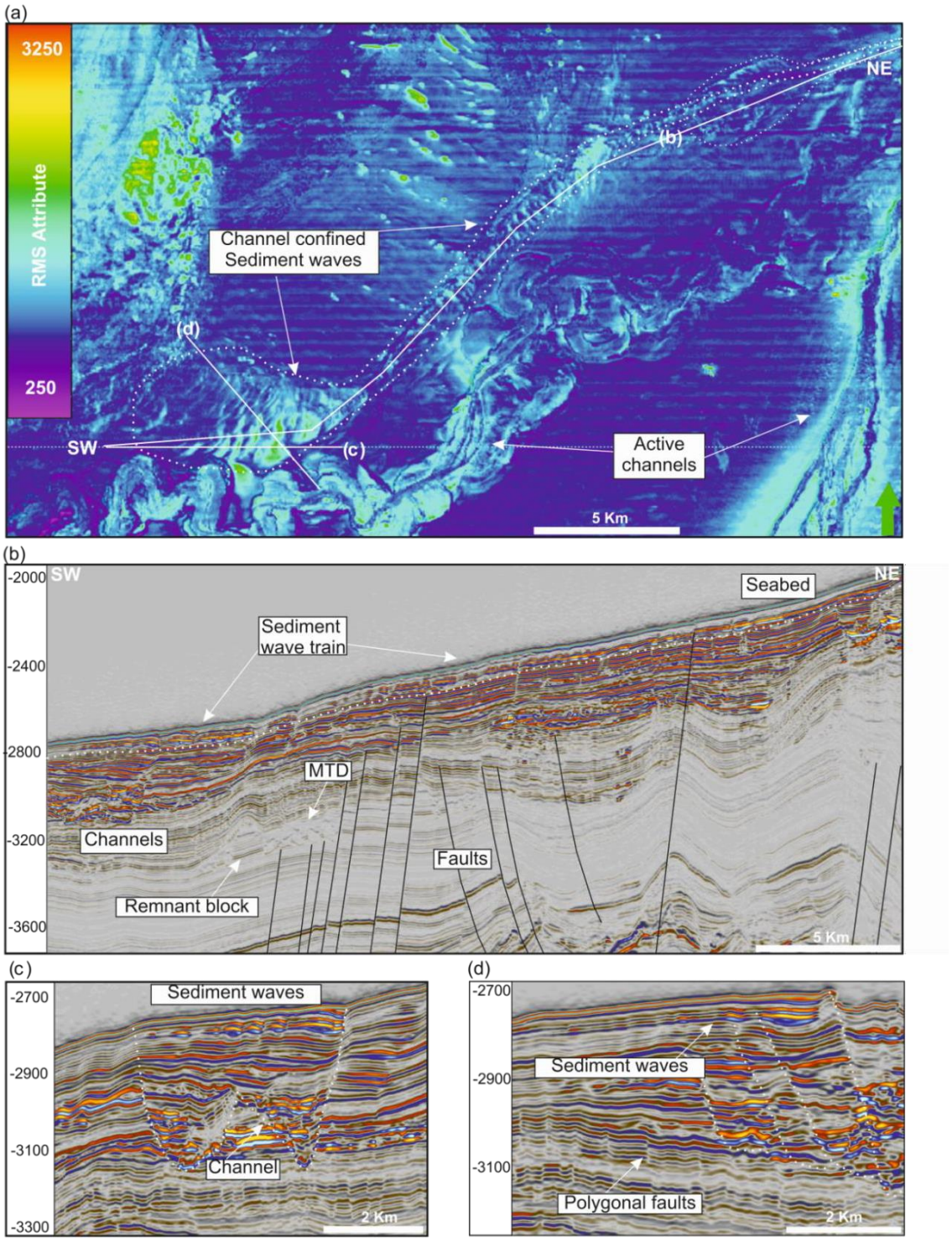
(a)
3250
RMS Attribute
250
NE
(b)
Channel confined
Sediment waves
(d)
SW
(c)
Active
channels
5 Km
(b)
-2000
SW
Seabed
NE
Sediment
wave train
-2400
-2800
MTD
-3200
Channels
Faults
Remnant block
-3600
5 Km
(c)
-2700
Sediment waves
-2900
-3100
Channel
-3300
2 Km
(d)
-2700
Sediment waves
-2900
-3100
Polygonal faults
2 Km

Fig. 13.

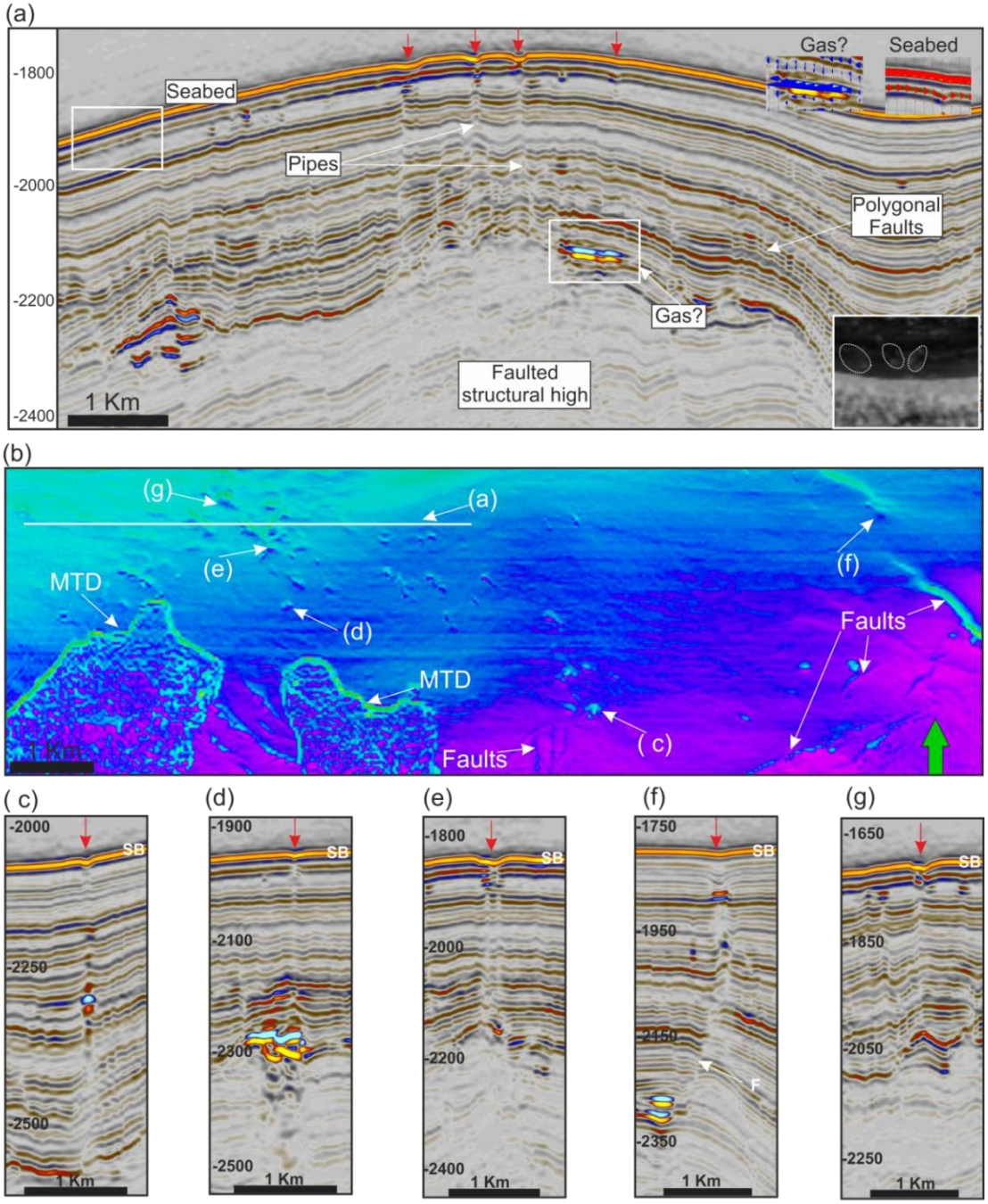
(a)
-1800
-2000
-2200
-2400
Seabed
Pipes
Gas?
Seabed
Polygonal Faults
Gas?
Faulted structural high
1 Km
(b)
(g)
(a)
(e)
MTD
(d)
MTD
(f)
Faults
Faults
(c)
1 Km
(c)
-2000
SB
-2250
-2500
1 Km
(d)
-1900
SB
-2100
-2300
-2500
1 Km
(e)
-1800
SB
-2000
-2200
-2400
1 Km
(f)
-1750
SB
-1950
-2150
F
-2350
1 Km
(g)
-1650
SB
-1850
-2050
-2250
1 Km

Fig. 14.

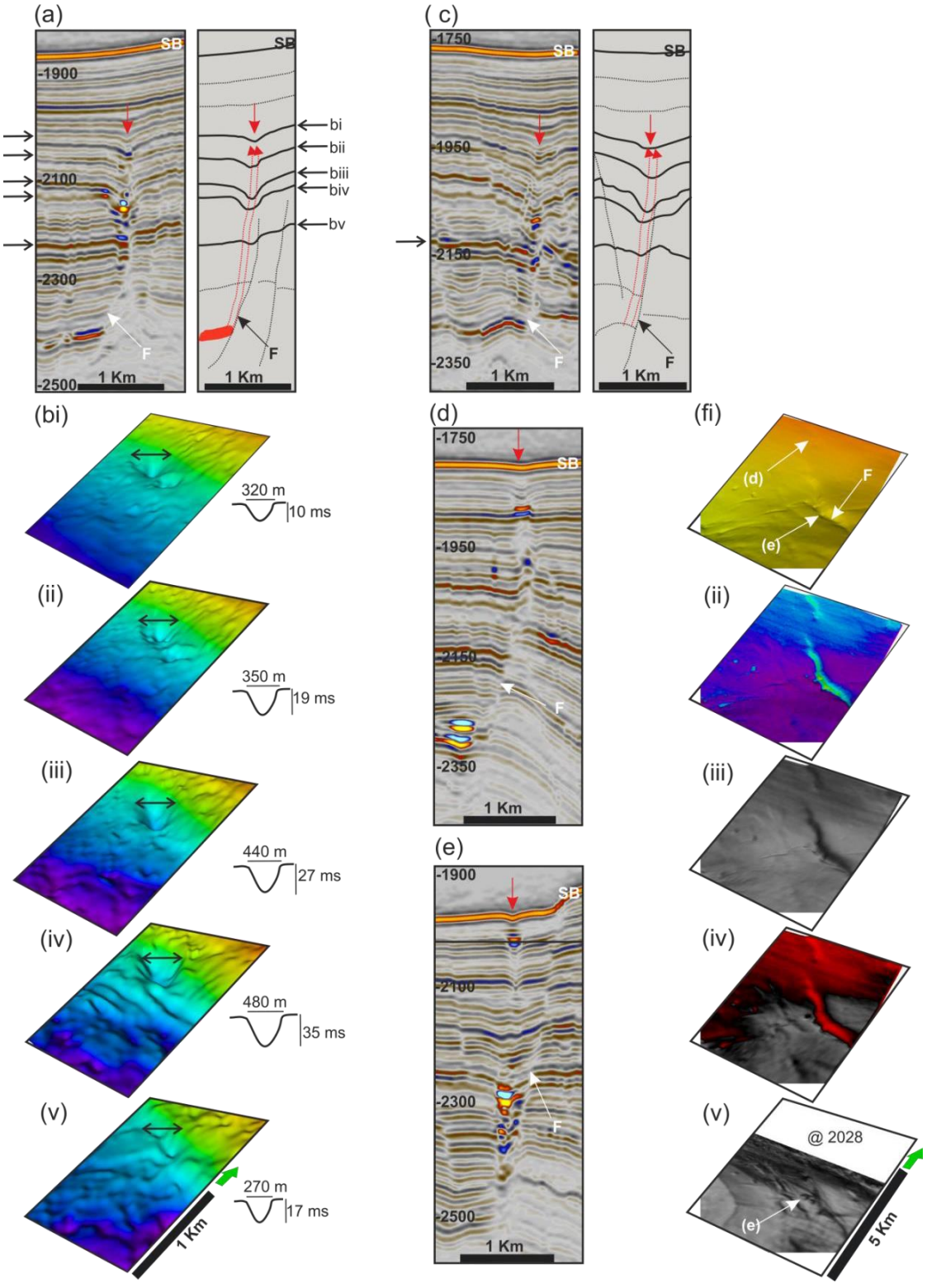
(a)
SB
-1900
-2100
-2300
-2500
F
1 Km
bi
bii
biii
biv
bv
(c)
-1750
-1950
-2150
-2350
(bi)
320 m
10 ms
(ii)
350 m
19 ms
(iii)
440 m
27 ms
(iv)
480 m
35 ms
(v)
270 m
17 ms
(d)
(e)
(fi)
@ 2028
5 Km

Fig.15.

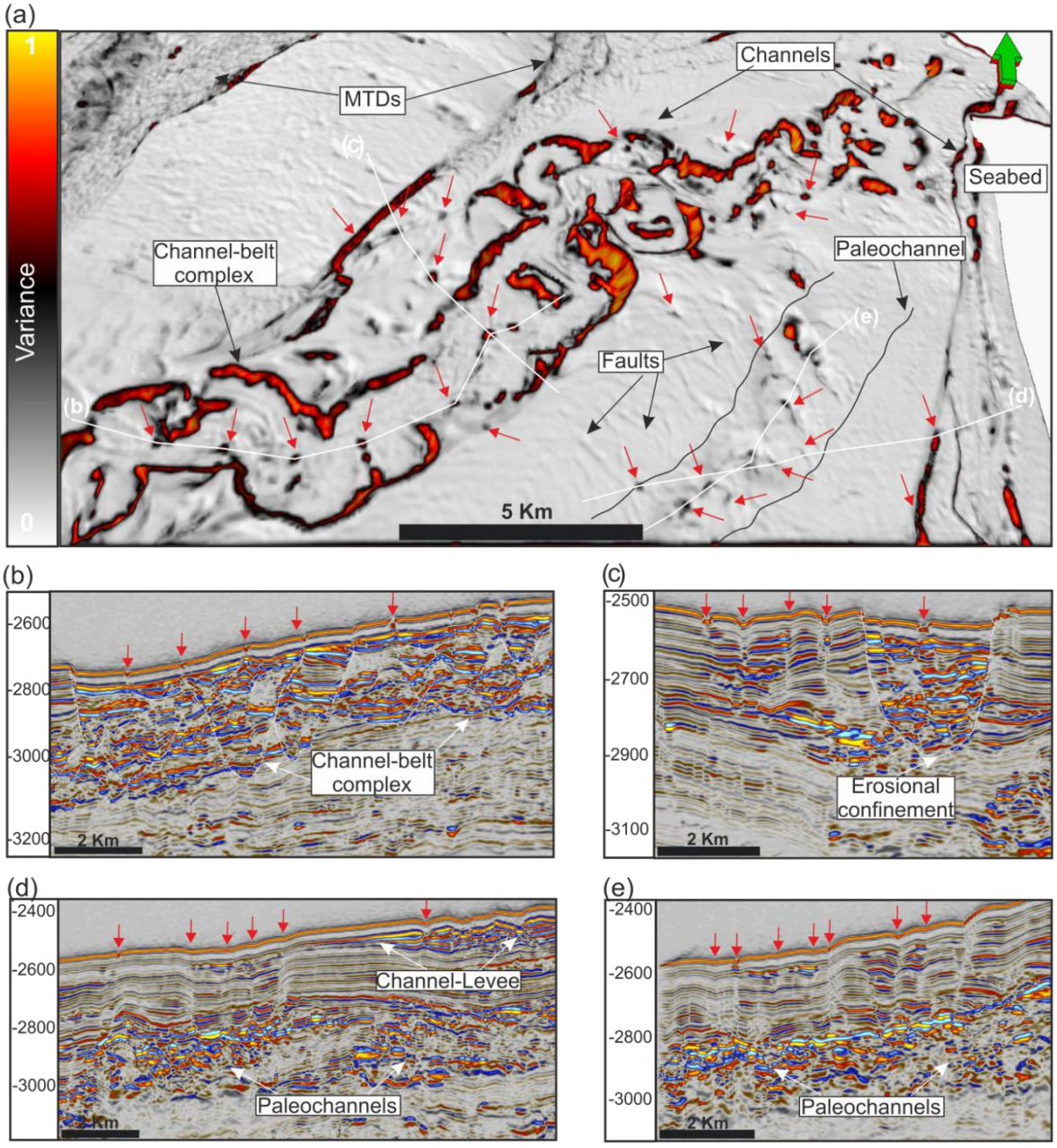
(a)
1
Variance
0
MTDs
Channels
Seabed
Channel-belt complex
Paleochannel
Faults
(b)
(c)
(d)
(e)
5 Km
(b)
-2600
-2800
-3000
-3200
Channel-belt complex
2 Km
(c)
-2500
-2700
-2900
-3100
Erosional confinement
2 Km
(d)
-2400
-2600
-2800
-3000
Channel-Levee
Paleochannels
2 Km
(e)
-2400
-2600
-2800
-3000
Paleochannels
2 Km

Fig. 16

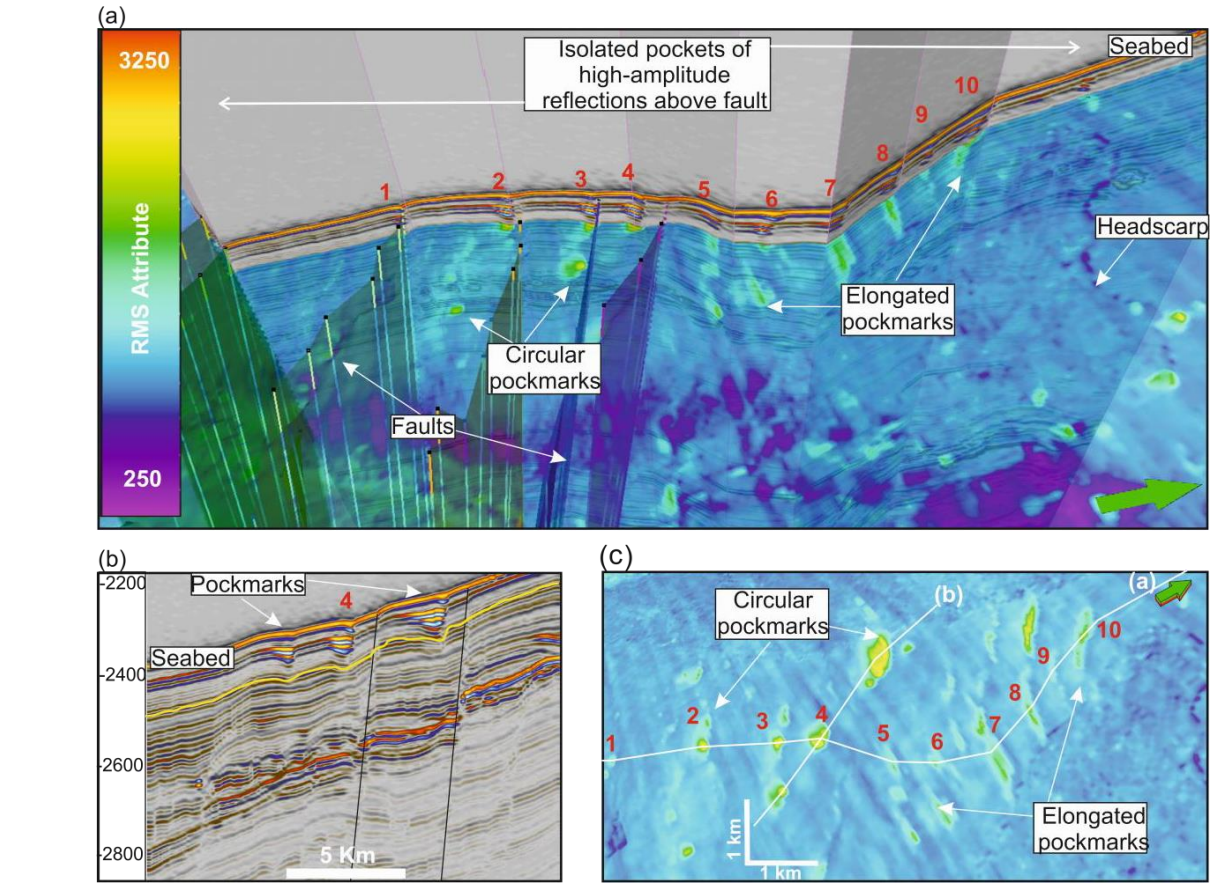
(a)
3250
RMS Attribute
250
Isolated pockets of high-amplitude reflections above fault
Seabed
Headscarp
Elongated pockmarks
Circular pockmarks
Faults
(b)
Pockmarks
Seabed
5 Km
(c)
Circular pockmarks
Elongated pockmarks
1 km
1 km

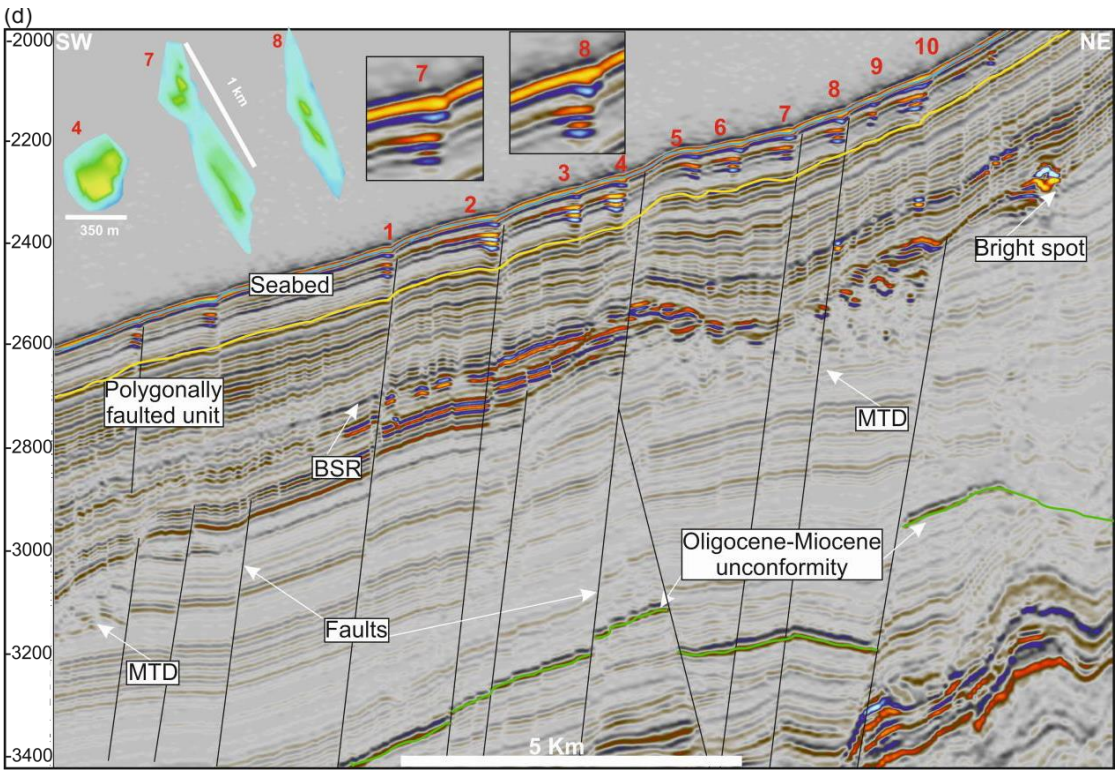
(d)
SW
NE
Seabed
Polygonally faulted unit
BSR
MTD
Bright spot
Oligocene-Miocene unconformity
Faults
MTD
350 m
1 km
5 Km

Fig. 17

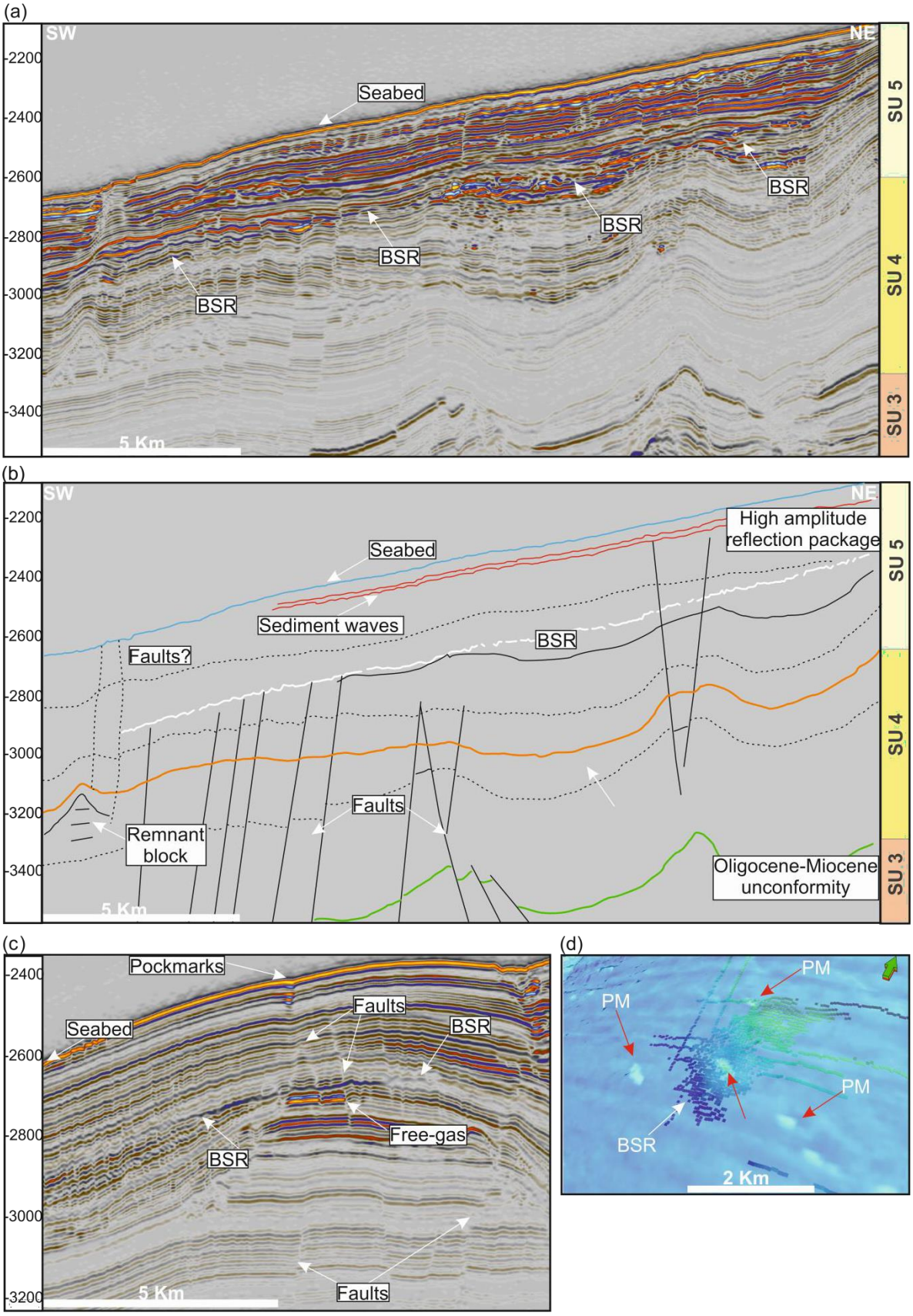
(a)
SW
NE
-2200
-2400
-2600
-2800
-3000
-3200
-3400
Seabed
BSR
BSR
BSR
BSR
5 Km
SU 5
SU 4
SU 3
(b)
SW
NE
-2200
-2400
-2600
-2800
-3000
-3200
-3400
Seabed
Sediment waves
Faults?
BSR
High amplitude reflection package
Faults
Remnant block
Oligocene-Miocene unconformity
5 Km
SU 5
SU 4
SU 3
(c)
-2400
-2600
-2800
-3000
-3200
Pockmarks
Seabed
Faults
BSR
BSR
Free-gas
Faults
5 Km
(d)
PM
PM
PM
BSR
2 Km

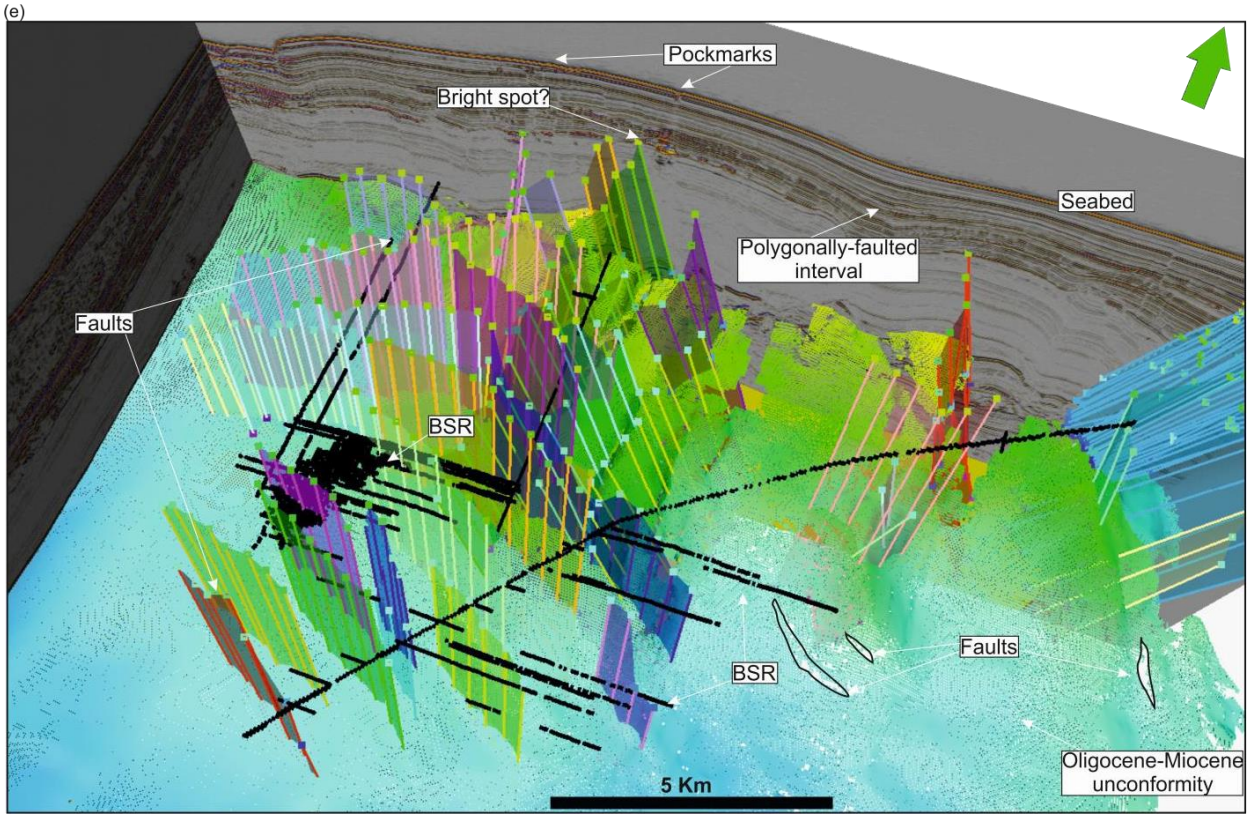
(e)
Pockmarks
Bright spot?
Seabed
Polygonally-faulted interval
Faults
BSR
BSR
Faults
Oligocene-Miocene unconformity
5 Km

Fig. 18

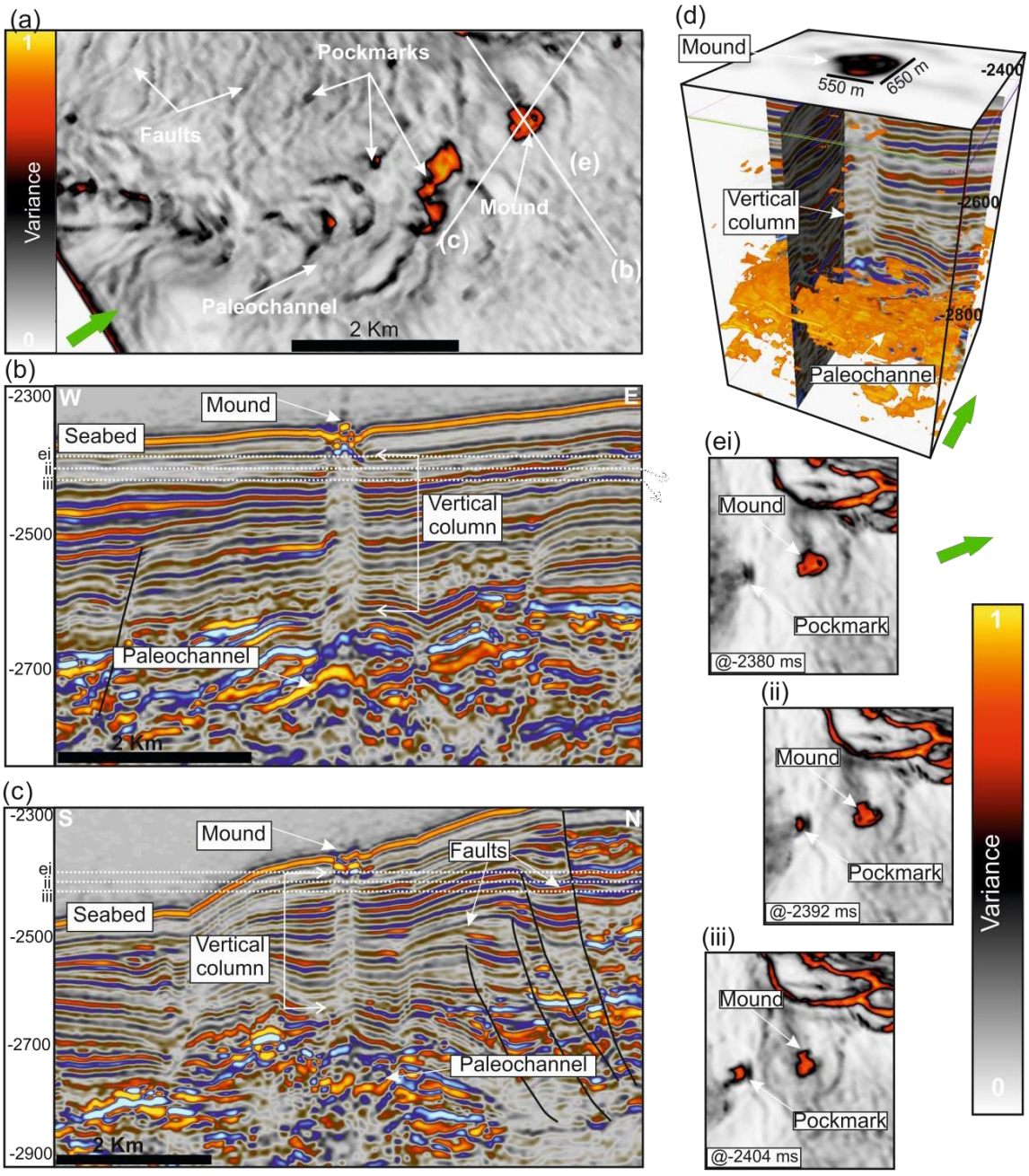
(a)
Variance
1
0
Pockmarks
Faults
(e)
Mound
(c)
(b)
Paleochannel
2 Km
(b)
-2300
W
E
Mound
Seabed
ei
ii
iii
-2500
Vertical column
-2700
Paleochannel
2 Km
(c)
-2300
S
N
Mound
Faults
ei
ii
iii
Seabed
-2500
Vertical column
-2700
Paleochannel
2 Km
-2900
(d)
Mound
550 m
650 m
-2400
Vertical column
-2600
-2800
Paleochannel
(ei)
Mound
Pockmark
@-2380 ms
(ii)
Mound
Pockmark
@-2392 ms
(iii)
Mound
Pockmark
@-2404 ms
1
Variance
0

Fig.19.

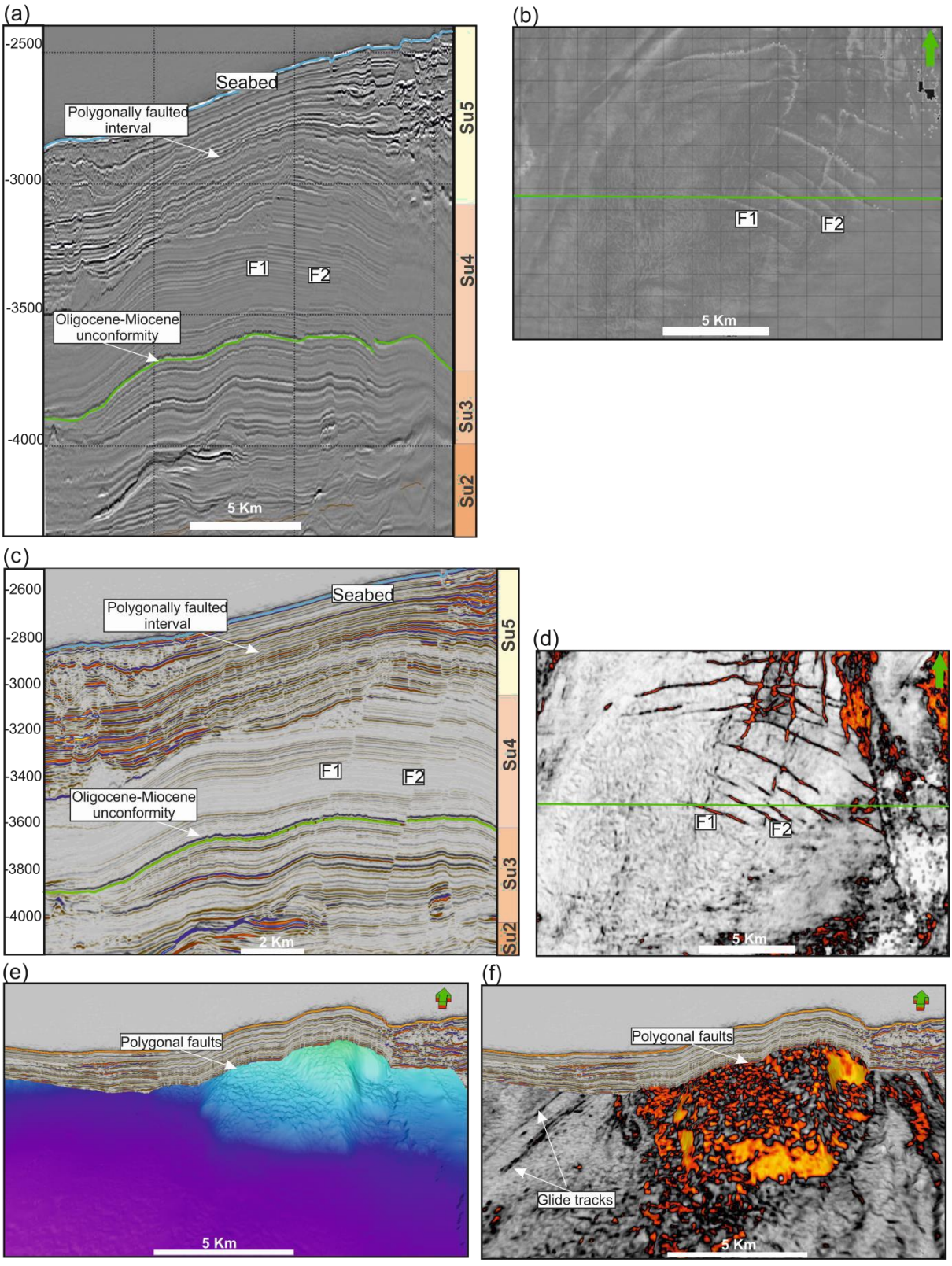
(a)
-2500
-3000
-3500
-4000
Seabed
Polygonally faulted interval
F1
F2
Oligocene-Miocene unconformity
5 Km
Su5
Su4
Su3
Su2
(b)
F1
F2
5 Km
(c)
-2600
-2800
-3000
-3200
-3400
-3600
-3800
-4000
Seabed
Polygonally faulted interval
F1
F2
Oligocene-Miocene unconformity
2 Km
Su5
Su4
Su3
Su2
(d)
F1
F2
5 Km
(e)
Polygonal faults
5 Km
(f)
Polygonal faults
Glide tracks
5 Km

Fig 20.

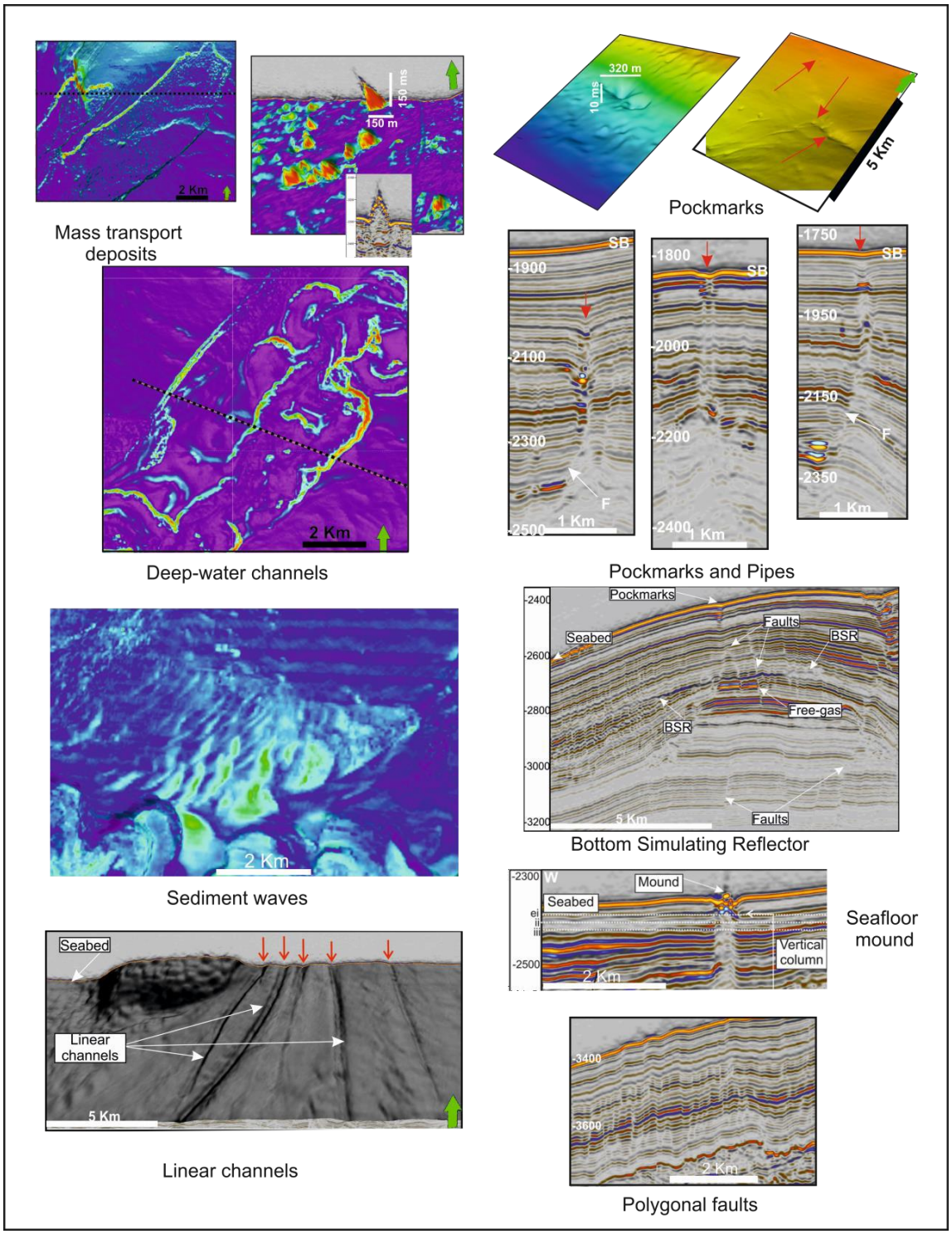
2 Km
150 m
150 ms
Mass transport deposits
320 m
10 ms
5 Km
Pockmarks
SB
-1900
-2100
-2300
-2500
F
1 Km
-1800
-2000
-2200
-2400
-1750
-1950
-2150
-2350
Pockmarks and Pipes
2 Km
Deep-water channels
Pockmarks
Seabed
Faults
BSR
Free-gas
-2400
-2600
-2800
-3000
-3200
5 Km
Bottom Simulating Reflector
2 Km
Sediment waves
-2300
W
Mound
Seabed
ei
ii
iii
-2500
Vertical column
2 Km
Seafloor mound
Seabed
Linear channels
5 Km
Linear channels
-3400
-3600
2 Km
Polygonal faults

Fig. 21

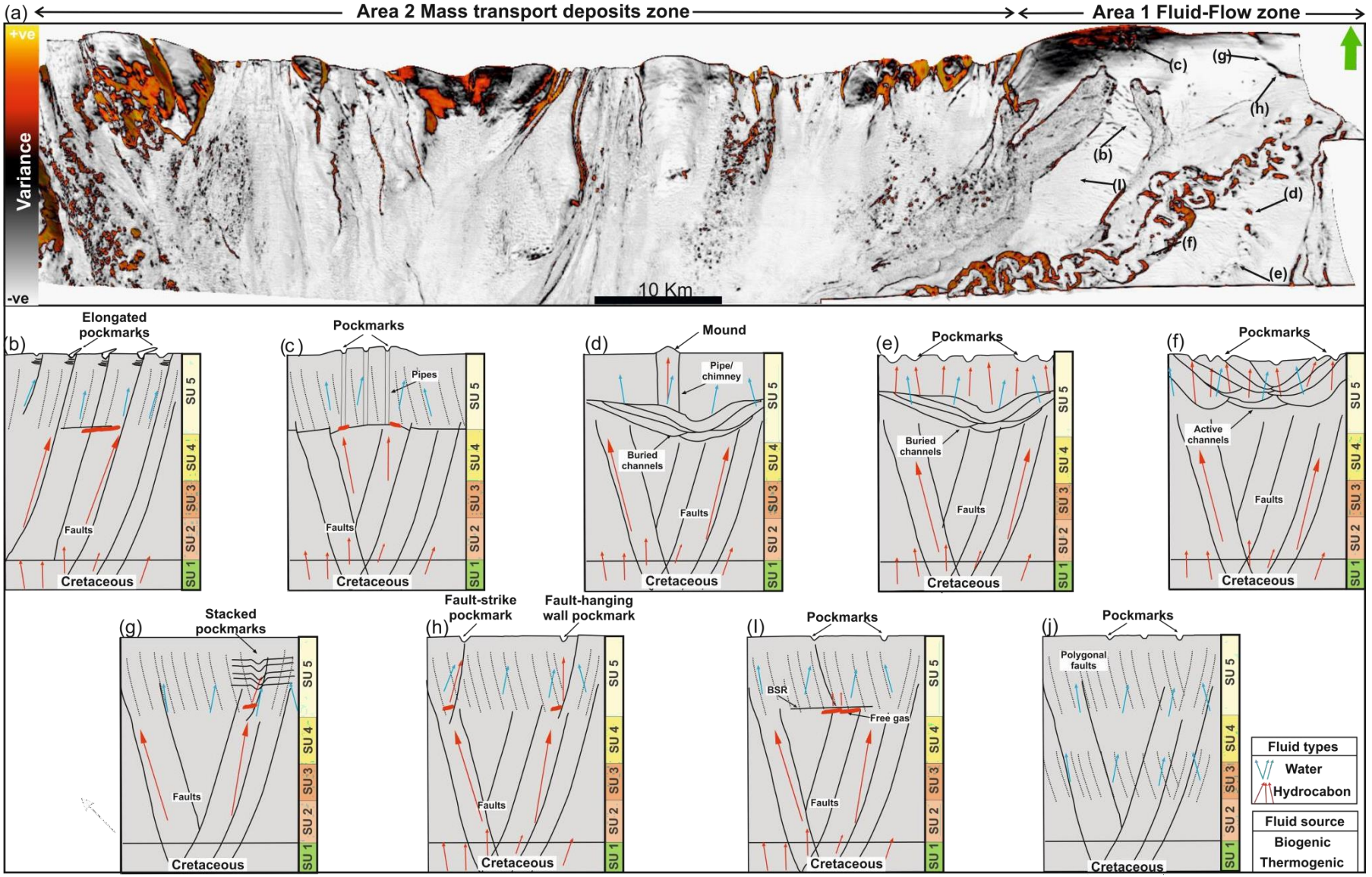
(a)
Area 2 Mass transport deposits zone
Area 1 Fluid-Flow zone
+ve
Variance
-ve
10 Km
(b)
(c)
(d)
(e)
(f)
(g)
(h)
(l)
(j)
Elongated pockmarks
Pockmarks
Pipes
Mound
Pipe/ chimney
Buried channels
Active channels
Faults
Cretaceous
SU 1
SU 2
SU 3
SU 4
SU 5
Stacked pockmarks
Fault-strike pockmark
Fault-hanging wall pockmark
BSR
Free gas
Polygonal faults
Fluid types
Water
Hydrocabon
Fluid source
Biogenic
Thermogenic

Fig. 22

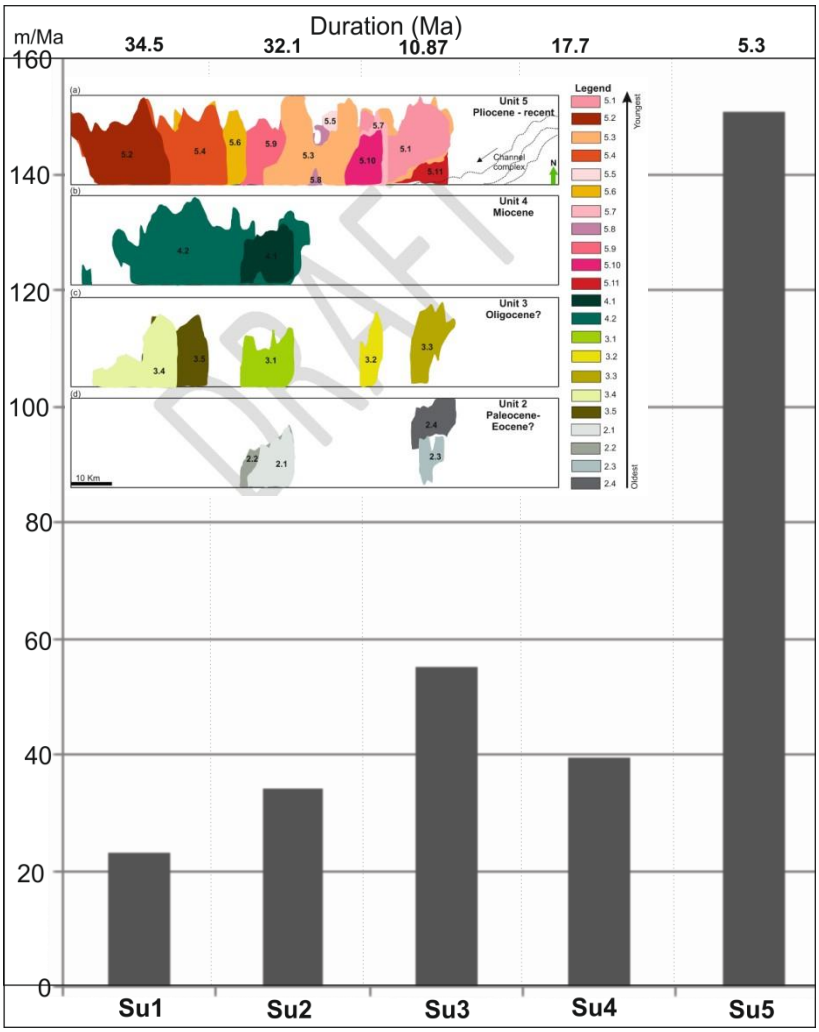
Duration (Ma)
m/Ma
34.5
32.1
10.87
17.7
5.3
160
140
120
100
80
60
40
20
0
Unit 5
Pliocene - recent
Unit 4
Miocene
Unit 3
Oligocene?
Unit 2
Paleocene-
Eocene?
Channel complex
N
10 Km
Legend
Youngest
Oldest
Su1
Su2
Su3
Su4
Su5

Fig. 23

SEISMIC UNITS	FREQUENCY (hz)	INTERVAL VELOCITIES (km/s)	HORIZONTAL RESOLUTION (m)	VERTICAL RESOLUTION (m)
SU1	25	2	42	20
SU2	48	2	21	10
SU3	30	2	33	17
SU4	40	2	25	13
SU5	50	2	20	10

Table 1

BASIN EXAMPLE	2D GEOMETRY	PLAN VIEW GEOMETRY	FAULT THROW (M)	RANGE/AV FAULT DIP (º)	AUTHORS
Central North Sea	Normal faults	Distinctly Polygonal	NA	30 – 70 (45)	Cartwright & Lonergan 1996
Central North Sea	Normal faults	Distinctly Polygonal	8 – 100	27 – 67 (45)	Lonergan *et al.,* 1998
Northern North Sea	Normal faults	Distinctly Polygonal	8 – 30	31 – 56	Olobayo *et al.,* 2015
Faroe-Shetland Basin	Normal faults	Distinctly Polygonal	NA	55 – 85 (58 +/-2)	Shoulders *et al.,* 2007
Faroe-Shetland Basin	Normal faults	Distinctly Polygonal	NA	Type 2a – 63 Type 3 - 68	Bureau *et al.,* 2013
More Basin	Normal faults	Distinctly Polygonal	Few metres to 80	25 - 50	Stuevold *et al.,* 2003
Lower Congo Basin	Normal faults	Distinctly Polygonal	5 - 20	NA	Gay *et al.,* 2004
Nigeria Transform Margin	**Normal faults**	**Slightly polygonal**	**3-11**	**41 – 50 (46)**	**This study**

Table 2

SEISMIC UNITS	SERIES	DURATION (Ma)	THICKNESS (ms) max	VELOCITY (Km/s)	NET ACC. RATE (m/Ma) max
SU1	Late Cretaceous	34.5	800	2	23.2
SU2	Paleocene-Eocene?	32.1	1100	2	34.3
SU3	Oligocene?	10.87	700	2	55.2
SU4	Miocene?	17.7	900	2	39.5
SU5	Pliocene to date?	5.3	1100	2	150.9

Table 3